CR 91.008

NCEL

Contract Report

July 1991

CEMCOM Research Associates, Inc.
and
University of Maryland

A MECHANISTIC STUDY OF FAILURE OF CONCRETE SUBJECTED TO CYCLIC THERMAL LOADS

ABSTRACT The report describes a study to investigate mechanisms which lead to fatigue failure of concrete pavement surfaces due to their repeated exposure to the hot exhaust gases of the auxiliary power unit (APU) of F/A-18 aircraft. The experimental results show a degradation of the microstructure and the mechanical properties with thermal cycling. Analytical modeling was used to calculate temperature and stress distributions in a concrete which is heated on the surface by a hot air stream. From the analysis and discussion of the results, a hypothesis for a heat fatigue failure mechanism was developed. This mechanism is the creation and propagation of microcracks in the concrete. The cracks are mostly caused by drying shrinkage and lead to a scaling of the concrete surface. Four methods are proposed to modify concretes to achieve a better heat resistance when exposed to thermal cycling.

NAVAL CIVIL ENGINEERING LABORATORY PORT HUENEME CALIFORNIA 93043

METRIC CONVERSION FACTORS

Approximate Conversions to Metric Measures

Symbol	When You Know	Multiply by	To Find	Symbol
		LENGTH		
in	inches	*2.5	centimeters	cm
ft	feet	30	centimeters	cm
yd	yards	0.9	meters	m
mi	miles	1.6	kilometers	km
		AREA		
in^2	square inches	6.5	square centimeters	cm^2
ft^2	square feet	0.09	square meters	m^2
yd^2	square yards	0.8	square meters	m^2
mi^2	square miles	2.6	square kilometers	km^2
	acres	0.4	hectares	ha
		MASS (weight)		
oz	ounces	28	grams	g
lb	pounds	0.45	kilograms	kg
	short tons (2,000 lb)	0.9	tonnes	t
		VOLUME		
tsp	teaspoons	5	milliliters	ml
Tbsp	tablespoons	15	milliliters	ml
fl oz	fluid ounces	30	milliliters	ml
c	cups	0.24	liters	l
pt	pints	0.47	liters	l
qt	quarts	0.95	liters	l
gal	gallons	3.8	liters	l
ft^3	cubic feet	0.03	cubic meters	m^3
yd^3	cubic yards	0.76	cubic meters	m^3
		TEMPERATURE (exact)		
°F	Fahrenheit temperature	5/9 (after subtracting 32)	Celsius temperature	°C

*1 in = 2.54 (exactly). For other exact conversions and more detailed tables, see NBS Misc. Publ. 286, Units of Weights and Measures, Price $2.25, SD Catalog No. C13.10:286.

Approximate Conversions from Metric Measures

Symbol	When You Know	Multiply by	To Find	Symbol
		LENGTH		
mm	millimeters	0.04	inches	in
cm	centimeters	0.4	inches	in
m	meters	3.3	feet	ft
m	meters	1.1	yards	yd
km	kilometers	0.6	miles	mi
		AREA		
cm^2	square centimeters	0.16	square inches	in^2
m^2	square meters	1.2	square yards	yd^2
km^2	square kilometers	0.4	square miles	mi^2
ha	hectares (10,000 m^2)	2.5	acres	
		MASS (weight)		
g	grams	0.035	ounces	oz
kg	kilograms	2.2	pounds	lb
t	tonnes (1,000 kg)	1.1	short tons	
		VOLUME		
ml	milliliters	0.03	fluid ounces	fl oz
l	liters	2.1	pints	pt
l	liters	1.06	quarts	qt
l	liters	0.26	gallons	gal
m^3	cubic meters	35	cubic feet	ft^3
m^3	cubic meters	1.3	cubic yards	yd^3
		TEMPERATURE (exact)		
°C	Celsius temperature	9/5 (then add 32)	Fahrenheit temperature	°F

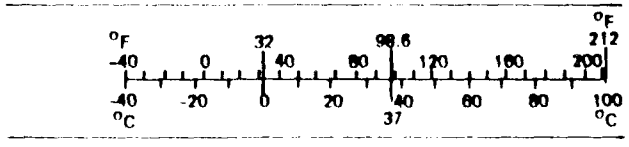

DISCLAIMER NOTICE

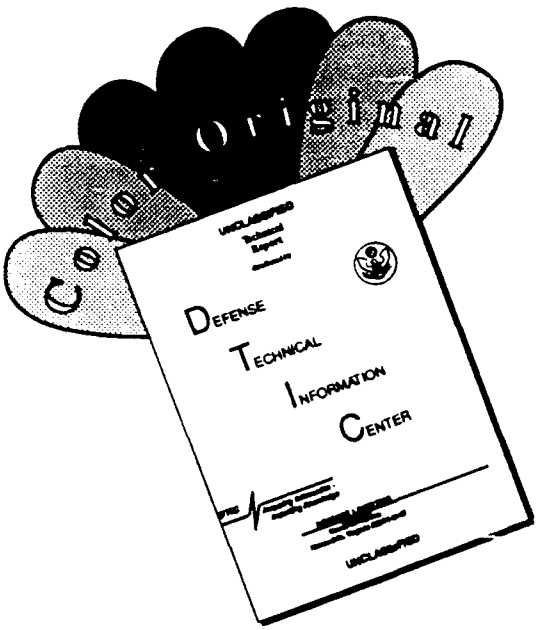

THIS DOCUMENT IS BEST QUALITY AVAILABLE. THE COPY FURNISHED TO DTIC CONTAINED A SIGNIFICANT NUMBER OF COLOR PAGES WHICH DO NOT REPRODUCE LEGIBLY ON BLACK AND WHITE MICROFICHE.

REPORT DOCUMENTATION PAGE

Form Approved
OMB No. 0704-018

1. AGENCY USE ONLY *(Leave blank)*	2. REPORT DATE	3. REPORT TYPE AND DATES COVERED
	July 1991	Final; May 1990 through February 1991

4. TITLE AND SUBTITLE

A MECHANISTIC STUDY OF FAILURE OF CONCRETE SUBJECTED TO CYCLIC THERMAL LOADS

5. FUNDING NUMBERS

PE - 0605502
PR - Y2016
C - N47408-90-C-1147

6. AUTHOR(S)

Dr. Thomas A. Bier,* Dr. Sean Wise,* and
Dr. Peter Chang**

7. PERFORMING ORGANIZATION NAME(S) AND ADDRESS(ES)

CEMCOM Research Associates, Inc.*
10123 Senate Drive
Lanham, MD 20706

Department of Civil Engineering**
University of Maryland
College Park, MD 20742

8. PERFORMING ORGANIZATION REPORT NUMBER

CR 91.008

9. SPONSORING/MONITORING AGENCY NAME(S) AND ADDRESS(ES)

Naval Civil Engineering Laboratory
Code L53
Port Hueneme, CA 93043-5003

10. SPONSORING/MONITORING AGENCY REPORT NUMBER

11. SUPPLEMENTARY NOTES

12a. DISTRIBUTION/AVAILABILITY STATEMENT

Approved for public release; distribution is unlimited.

12b. DISTRIBUTION CODE

13. ABSTRACT *(Maximum 200 words)*

The report describes a study to investigate mechanisms which lead to fatigue failure of concrete pavement surfaces due to their repeated exposure to the hot exhaust gases of the auxiliary power unit (APU) of F/A-18 aircraft. The experimental results show a degradation of the microstructure and the mechanical properties with thermal cycling. Analytical modeling was used to calculate temperature and stress distributions in a concrete which is heated on the surface by a hot air stream. From the analysis and discussion of the results, a hypothesis for a heat fatigue failure mechanism was developed. This mechanism is the creation and propagation of microcracks in the concrete. The cracks are mostly caused by drying shrinkage and lead to a scaling of the concrete surface. Four methods are proposed to modify concretes to achieve a better heat resistance when exposed to thermal cycling.

14. SUBJECT TERMS

Concrete pavement surfaces, fatigure failure, aircraft exhaust gases, auxiliary power unit, thermal cycling,

15. NUMBER OF PAGES

65

16. PRICE CODE

17. SECURITY CLASSIFICATION OF REPORT	18. SECURITY CLASSIFICATION OF THIS PAGE	19. SECURITY CLASSIFICATION OF ABSTRACT	20. LIMITATION OF ABSTRACT
Unclassified	Unclassified	Unclassified	UL

FOREWORD

This project was aimed at understanding the behavior of normal weight (NW) concrete subjected to cyclic thermal loading. It includes experimental and analytical work with emphasis on thermal strain incompatibilities between cement paste and aggregates due to different coefficients of thermal expansion (CTE).

In the experimental work, the ability in determining material properties such as CTE and pore structure is commended. With respect to the APU exhaust simulation, it appears that although the exhaust gas temperature was duplicated, no attempt at reproducing the heat flow itself was made. The heat flow depends upon the air speed and the relative heat capacity. Actual heat flow is most likely higher given the high exhaust gas speed and probably higher specific heat. Although this simulation is not completely accurate nor conservative, it nonetheless yields an approximation to the concrete surface temperature gradient which is the basis for the concurrent analytical work. The experiment also shows that this gradient is indeed significantly lower than the exhaust gases temperature gradient.

The analytical model is a two-step procedure which determines heat distribution then stress field, very similar to previous NCEL work. The insight into stress concentrations at the cement paste-aggregate interface emphasizes one of the main problems with NW concretes. Mitigation of shrinkage effects is also a valuable proposition.

One shortcoming perhaps of Phase I is that the objective did not include the evaluation of the effects of other material parameters such as modulus of elasticity, unit weight, specific heat, and conductivity on the concrete heat resistance. While the recommendations for future work are very pertinent, less emphasis should be placed on further studying the behavior of materials that will fail (such as lower quality concrete) and more on how to determine heat resistant ones. The study of the aggregate-cement paste interface should not be directed towards further refinement but instead towards evaluating acceptable levels of CTE variation between aggregates and paste, which in turn would help with selecting acceptable aggregates.

In summary, this report provides useful new insight in the behavior of NW concrete subjected to thermal cycling.

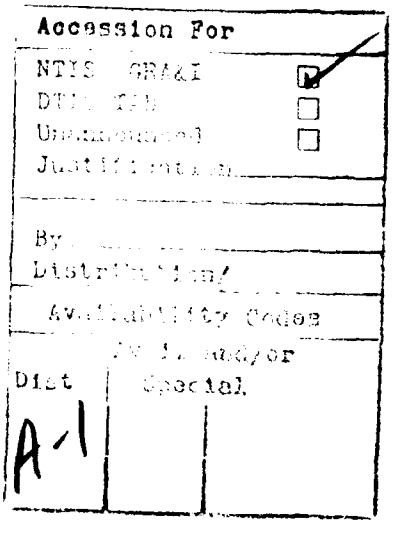

TABLE OF CONTENTS

LIST OF FIGURES

LIST OF TABLES

TABLE OF ABBREVIATIONS

APU	Auxillary Power Unit
CBC	Chemically Bonded Ceramic
CTE	Coefficient of Thermal Expansion
FEA	Finite Element Analysis
FEM	Finite Element Modeling
MIPS	Mercury Intrusion Pore Symmetry
NAS	Naval Air Station
NCEL	Naval Civic Engineering Laboratory
OPC	Ordinary Portland Cement
r.h.	Relative Humidity

Introduction

Airfield pavements are subjected to extremely severe use conditions. They must repeatedly resist dynamic loads induced by high speed, high performance aircraft which may weigh upwards of 70,000 lbs. for fighters, and 800,000 lbs. for transports (12). In addition, these pavements must survive severe weathering and resist attack from harsh deicing chemicals, jet fuels and hydraulic fluids. These pavements must now resist a new thermal threat of turbine exhaust, either from the APU (such as the F/A-18), sustained intense heat from vertical takeoff and landing aircraft (such as the AV-8B Harrier Jump Jet or the V-22 Osprey), and the brief but still higher temperatures resulting from vectored thrust of the next generation aircraft.

The US Navy has already experienced problems with concrete pavements in apron areas where F/A-18 fighter jets are stationed. The problem occurred after 1-2 years of service as a scaling of the concrete surface at locations where the hot exhaust gases of the APU hit the pavement. The heat exposure partially combined with oil and/or fuel spills seemed to be the cause of the failure.

The study described in this report was undertaken to understand mechanisms which lead to failure of pavements in F/A-18 parking areas. At the time the proposal was written the failure caused by the F/A-18's APU was thought to be the same type as experienced with AV-8B Harrier aircraft - an explosive spalling failure as it is experienced when concrete is heated too quickly (1,5).

During the planning phase of the project, however, it became apparent that the damage to pavements of Navy Airfields follows a different pattern. Mel Hironaka from NCEL, Port Hueneme, CA visited CEMCOM on May 18, 1990, and presented photographs from damaged parking areas as well as the experiments conducted so far by the Navy and their results. The damages looked like a scaling failure as opposed to a spalling failure. This means that instead of spalling explosively during one single heat exposure the concrete does not show damage until 1-2 years after it was regularly exposed to the APU's hot exhaust gases. By that time the concrete probably underwent hundreds of heat cycles. The failure is comparable to a freeze-thaw damage where visual degradation shows up only after enough freeze-thaw cycles. The damaged areas also looked very comparable to a concrete degraded by freezing and thawing.

With this new information the project had to be adjusted to look into a fatigue failure mechanism caused by cyclic thermal loading. Part of the original work plan

could be maintained but the emphasis shifted.

This report describes a study undertaken to understand the long term failure of concrete exposed to heat. It involves a literature search, experimental studies to investigate material parameters and characterization of microstructure, a simulation of the APU's impact on concrete and analytical models to calculate temperature and stress distributions in a concrete surface exposed to the hot APU exhaust gases.

Outline of the Project

The project started with a literature review. The review concentrated on three areas:

- temperature behavior of concrete.
- Naval studies of thermal failure of airfield parking aprons
- concrete microstructure especially bonding and microcracking.

The literature review provided data about mechanical and microstructural properties of concrete exposed to heat. These data, however, refer mostly to a one time heat exposure or only to spalling as opposed to scaling. Some literature was available about thermal cycling, long term heat exposure and microcracking - a possible fatigue mechanism - due to heating and cooling.

Therefore the first part of the experimental program concentrated on obtaining mechanical and microstructural properties on mortar specimens which underwent thermal cycling. The measurements focussed on development of strength and cracks as well as dimensional stability. It was suspected that the development of cracks is related to fatigue. Cracks form due to Coefficient Thermal Expansion (CTE) mismatch between aggregates and matrix and due to shrinkage, parameters which define the dimensional behavior of a solid.

The second part of the experimental program were experiments to simulate the APU's impact on a concrete pavement. Part of this was the design and construction of a hot air blower unit. The measurements themselves concentrated on getting temperature profiles on the surface and inside a concrete slab. According to the Navy's reports there seemed to be a need for data concerning the actual temperature load on and in the concrete pavements. Furthermore experiments were conducted to assess the damage in a heat exposed concrete surface before the actual scaling starts. For these tests the surface permeability was measured by a vacuum decay method.

Parallel to and interacting with the experimental work, analytical modeling was performed by Professor Peter Chang from the University of Maryland. The interaction with the experiments was such that experimentally determined properties (CTE's and shrinkage function) were used as input for part of the models.

The modeling concentrated on three areas. 1) Calculation of a temperature distribution in concrete from the APU's exhaust data; 2) calculation of stresses in concrete resulting from a transient heat flow. This was done with and without accounting for shrinkage; and 3) calculation of stresses in an interface (matrix-aggregate) as well as in the surrounding matrix and the aggregate itself.

Literature

Most published data concerning the behavior of concrete at elevated temperatures is in the context of fire damage and performance in nuclear reactor vessels. Temperatures investigated range up to 2000F. The concretes investigated were mainly quartz (gravel) and limestone concretes subject to hydrothermal heating (nuclear power plant containment) or drying conditions during the heating phase (fire) (1-4).

One of the best sources of information is a paper by Schneider (1). In this article, the changes that take place in concrete as it is heated are carefully delineated and documented. Dimensional changes as a function of temperature are reported for a typical Ordinary Portland Cement (OPC) cement matrix. A cement matrix containing sand, with a water/cement ratio of 0.5 will expand up to about 300F and show a CTE of about 6-7 ppm/F. Above this temperature, the cement phases dehydrate and substantial shrinkage takes place. A limestone aggregate has a CTE of approximately 2.5 ppm/F but its CTE increases above 700F. Quartz aggregates on the other hand, have a CTE of approximately 6.5 to 7 and it is fairly linear up to the inflection point in the quartz expansion at about 950F. The author points out that the large aggregates in concrete tend to dominate the thermal expansion coefficient of the cementitious composite.

All reports also give compressive and flexural strength data on concrete upon heating. If the concrete can dry during the heating process a loss in strength is observed for both limestone and quartz concrete. The strength loss increases with increasing temperature. In a range of up to about 400F a compressive strength retention or even a slight increase can be observed (1,3,4).

Concrete subjected to thermal cycling looses more strength according to (4) with an increasing number of cycles. The modulus of elasticity also goes down. This effect could not be observed by another researcher (3) who saw no significant effect of the number of thermal cycles on the strength drop. If concrete is not exposed to cycles but to a high temperature for long periods of time (up to 3 months) the strength loss increases with increasing exposure time (2). This effect was observed for temperatures higher than 167F.

Reducing the water-cement ratio increases the initial strength of concrete and according to (2), it also enhances the performance after heat exposure - the retention strengths are higher. Results for high strength concretes were recently published in a report by Diederichs, et al (5) which examines three high strength binders and their behavior at temperature. He found that the control portland cement (initial strength 4500 psi) had nearly complete strength retention up to 700F while binders containing fly ash, silica fume or slag, retained only 65% of their initial strength up to this temperature. The initial strength of these materials was substantially higher, however, averaging about 13,500 psi. The higher absolute values of the strength in these systems, even after exposure to elevated temperature to 700F is encouraging except for one aspect related to their performance in a fire and that is spalling. The high strength of these materials is achieved through substantial reduction in the matrix gel pore size. The decreased permeability does not allow diffusion of moisture rapidly enough to prevent failure.

In hydrothermal conditions, concrete also loses strength but this is much more severe for limestone concrete (2). The strength loss in these cases is attributed to mineralogical changes in the binder which lead to a coarsening of the pore structure (6). For quartz concrete these negative changes are compensated by an additional reaction of free silica and/or fine sand with calcium hydroxide (2), (6).

For concrete which dries during heat exposure, the damages result from the decrease in strength caused by the formation and propagation of cracks (7). For temperatures up to 662F cracking happens during the cooling phase, for temperatures above 842F the majority of cracking takes place during heat-up. Kordina et al. obtained these results from creep and acoustic emission measurements (7).

The more or less 'classic' literature does not contain any information about the bonding/interfacial behavior of aggregates and matrix. Bonding studies are limited to the

pull-out behavior of concrete reinforcement. Some limited information about the aggregate-matrix bond is available from a recent Materials Research Society Symposium on "Bonding in Cementitious Composites" (8).

TABLE I. Cleavage Strength of Composite Samples Prepared with Different Kinds of Cements and Rocks (Odler and Zurz) (8)

		Cleavage Strengths (psi)		
	Hydration Time	Basalt	Quartz	Limestone
OPC	1w*	73±30	87±30	145±30
	4w	101±15	116±58	189±15
	8w	116±15	174±44	203±58
	8w + 12 hr @ 200F	0	174±58	131±30
OPC + 10% Silica Fume	1w	174±58	174±58	160±30
	4w	232±73	247±73	218±44
	8w	247±73	290±87	261±58
	8w + 12 hr @ 200F	0	262±87	203±58
OPC + 5% PFA	1w	101±15	131±15	118±15
	4w	131±30	174±44	160±15
	8w	131±30	189±44	203±44
	8w + 12 hr @ 200F	0	203±44	174±44

*w = week

Table 1, is reproduced from a paper by Odler (8). It is interesting to note that the bond strength to limestone is better than quartzite when cured at room temperature. If well hydrated samples are heated to 200F in a moist environment, the quartzite bond strength does not change but the limestone bond strength is reduced by 35%. Pulverized Fly Ash (PFA) or silica fume can improve the bond strength in both cases. Other studies report bond strength 50% higher but the same relative trends hold (9).

It is interesting to note that the Navy reports authored by George Wu reflect a similar development as the general literature about temperature behavior of concrete. While most of these reports dealt with the higher exhaust temperatures of the AV-8B and the adv ..ed V/TOL, two of the reports (15, 17), dealt with the APU heating problem on the F/A-18. This shows that up to now there was no real need to study thermal, cyclic exposure of concrete. One apparent difficulty in studying this phenomena is the problem of getting consistent data. Experiments were carefully designed so that at each parking position, a

control was run on half the exhaust impingement area and a coating was tested on the other half. In most instances the control and the test section in an individual location would yield the same results yet big differences might be found from one parking position to the next.

Another important conclusion is the importance of the quality of the aggregates on the performance of the pavements, particularly when exposed to high temperature. Limestone aggregates were found to be the worst for heat resistance. The NAS Cecil Field parking aprons contained Florida limestone and has erosion or spalling in nearly all locations. The NAS Lemore parking aprons, which were made with concretes that had higher quality aggregates, showed much less heat induced damage. This information is consistent with the data found in our own literature search which is that the limestone aggregates to cement bond weakens when exposed to elevated temperature. The cause for this weakening has not been discussed in any of the literature that we have seen thus far. It could be that the surface bonding phase is thermally unstable and simply decomposes at high temperatures. Also, mismatch in CTE between the limestone and the sand filled cementitious binder might create a stress that leads to debonding.

Since the literature described in this section focuses more on the behavior of concrete exposed to relatively high temperatures for one cycle, there is not too much information available concerning a long term fatigue failure due to thermal cycling at lower temperatures. Therefore a rather intense part of the investigation was dedicated to experimental work in the area of material behavior at low temperature cycling (400F). This work is complimented by experiments on concrete (simulation of field exposure) and analytical calculations of temperature and stress distributions.

Experimental

Materials and Specimen Preparation

Mortar Samples

Five different mortars were cast using a Portland type I cement. All mixes had a ratio of water 4 parts: cement 10 parts: aggregate 25 parts. This corresponds to a paste: aggregate volume ratio of 1:3. The mix compositions are given in Table II.

TABLE II. Mix Composition for Mortars

Series #	Aggregate	Additives
1	Ottawa Sand (ASTM C-109)	M-100^R
2	Quartzite	M-100
3	Limestone	M-100
4	Quartzite	M-100 12% Silica Fume
5	Fused Silica	M-100

M-100^R is a high range water reducing admixture based on the sodium salt of beta-napthalene sulfonic acid, formaldehyde condensate. Quartz and limestone sand were locally available aggregates. The C-109 sand came from Ottawa, IL and the fused silica was a TECO fused silica from CE Minerals. The gradation of the aggregates was within the specifications for concrete sand according to ASTM C33.

The individual ingredients for a mix were dry mixed in a Hobert mixer for one minute, then water was added and mixing continued for another two minutes. Twelve bars, 6" x 1.5" x .75", twelve 2" cubes and two expansion bars 10" x 1" x 1" were cast from each mix. The samples were demolded after 24 hours and then cured in a moist box for 28 days.

Concrete Samples

Four concrete slabs 48" x 28" x 6" were cast using Portland cement type I and quartzite and limestone aggregate from the same sources as for the mortars. The maximum aggregate size was 3/4". The composition for the different slabs is given in Table III.

TABLE III. Composition for Concrete Slabs

Slab #	Aggregate	Additives
1	Quartz	M-100
2	Quartz	M-100
3	Quartz	M-100 Silica Fume
4	Limestone	M-100

All concretes had 610 lbs/yd.^{3} cement, 244 lbs/yd.^{3} water and 3241 lbs/yd.^{3} aggregate - the aggregates consisting of 1296 lbs/yd.^{3} sand and 1945 lbs/yd.^{3} gravel. The water cement ratio was 0.4.

The concrete was mixed in a 6.5 cu.ft. concrete mixer and placed into wooden frames sitting on a flat steel surface. On the bottom was a steel frame with reinforcement bars. Six thermocouples were also positioned inside the frame. Figure 1 shows a sketch of the concrete slab with the reinforcement cage and the thermocouples.

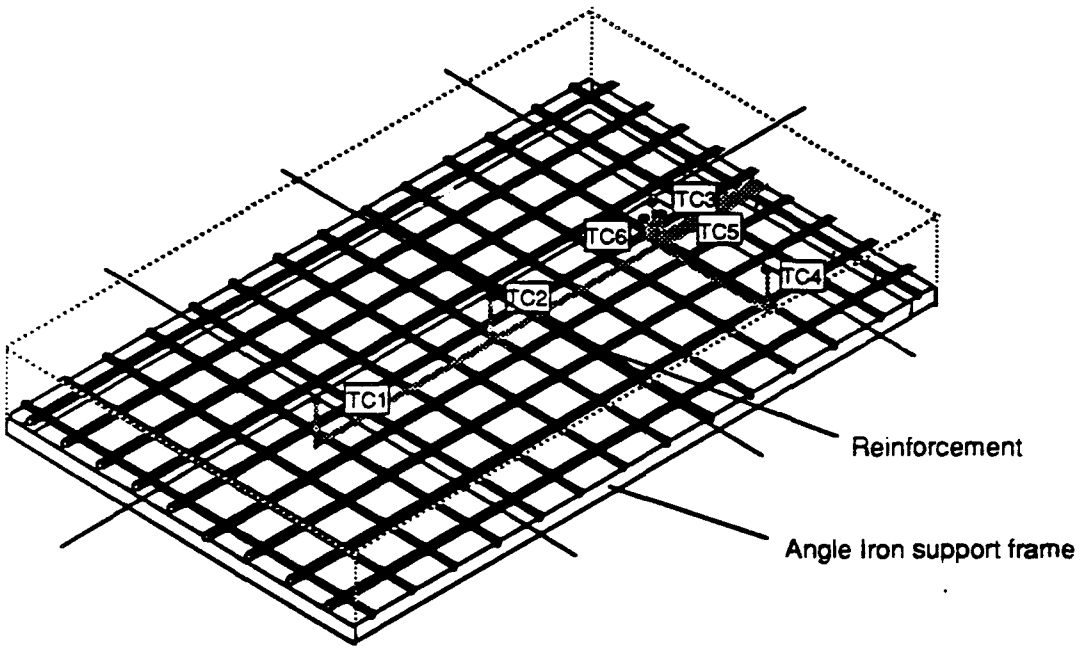

Figure 1. Concrete Slab with Reinforcement and Thermocouples

Thermocouples 1 through 4 were on the surface, thermocouples 5 and 6 under #3 at 1/2" and 1" depths, respectively. Thermocouple #3 was placed in the area of the hot air impingement.

After casting the concrete slab, surfaces were kept wet by spraying water on them. The slabs were wrapped in plastic and cured for 28 days.

Measurements

Mortar Sample Tests

After curing, the flexural strength and compressive strength was measured on three bars and cubes, respectively. The rest of the samples underwent heat cycling. One heat cycle consisted of placing the samples in an oven, which was at 400F for two hours, pulling them

out of the oven afterwards and letting them cool down for two hours at ambient temperature. Weights and lengths of the expansion bars were measured before and after the heat cycle.

After 1, 11 and 50 heat cycles, flexural and compressive strengths were determined.

Dilatometer experiments were carried out on separate specimens 2" x 1/2" x 1/2". While the length changes were measured the samples were heated to 400F at a rate of 35F/hr. After the first run all the moisture (free water) was lost and the shrinkage was determined. A second experiment was conducted right afterwards for the dry sample. This yielded the coefficient of thermal expansion (CTE). The CTE was used to calculate the shrinkage as a function of temperature from the first run. Figure 2 shows schematically the results from the dilatometer experiments.

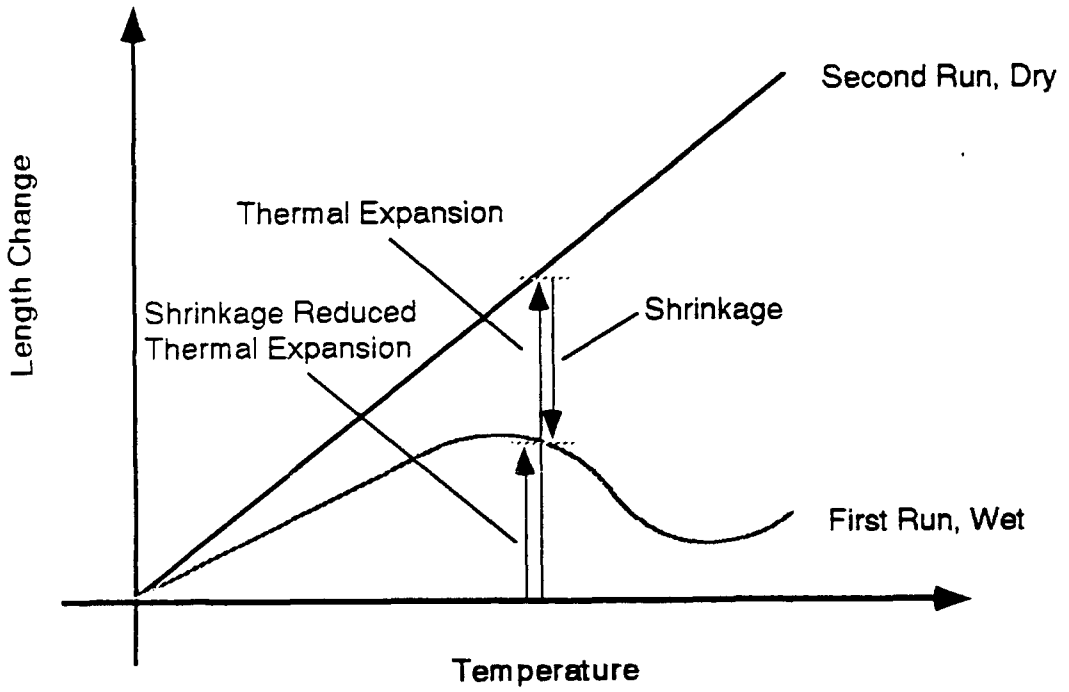

Figure 2. Schematic Dilatometer Traces for Wet and Dry Mortar Specimens

The pore structure was determined using mercury intrusion porosimetry (MIP). Mercury as a non-wetting fluid (contact angle >90 degrees) will not penetrate a pore system unless pressure is applied. Washburn deducted an equation which correlates the pressure necessary to fill a

cylindrical pore with its pore diameter (10):

$$p = \frac{4\sigma\cos\theta}{d}$$

where p = pressure
σ = surface tension for Hg
θ = contact angle
d = pore diameter

Figure 3 shows the principle of mercury penetrating a pore.

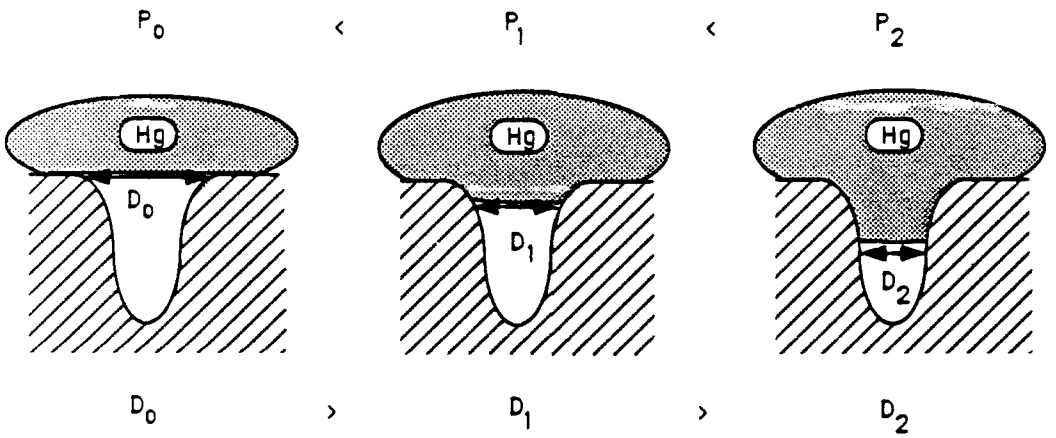

Figure 3. Principle of Mercury Intrusion Porosimetry (MIP)

During the measurement, the sample is surrounded by mercury. In the beginning, the pressure is very low and then increased. While the pressure increases, the volume of mercury intruding the sample is measured. The pressure-intruded volume measurements result in a cumulative volume distribution as shown in Figure 4. The coarse pore volume is measured first at low pressure and, as the pressure increases along with the intruded volume, the fine pore volume is measured. Therefore, even though the data is plotted from small pore on the left to large pore on the right, the actual measurement takes place from large to small or right to left.

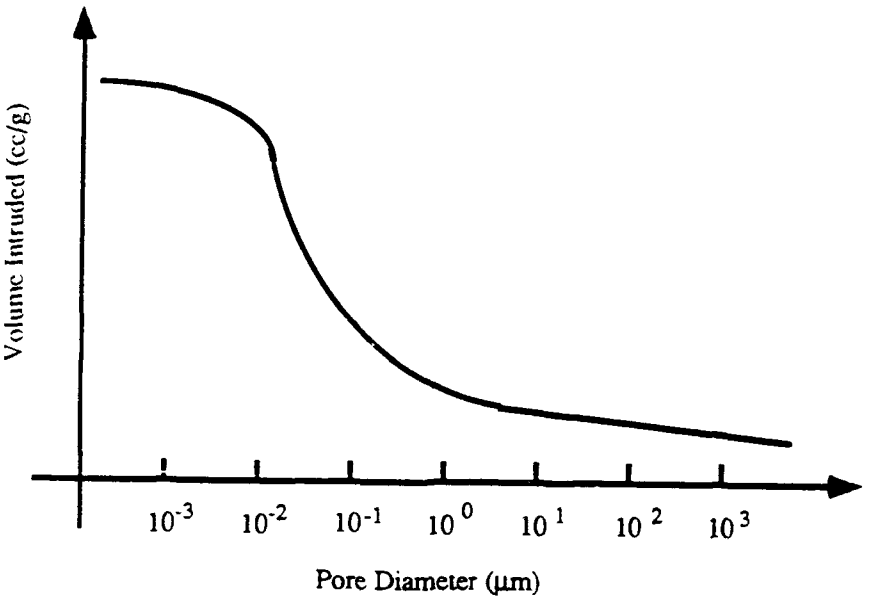

Figure 4. Schematic Cumulative Intruded Volume Distribution

For pressures between .5 psi and 60,000 psi a pore diameter range between 300 um and $2*10^{-3}$ um is accessible during the measurement.

MIP measurements were done for the control samples and the heat cycled samples. Parts of the flex bars were used.

Concrete Sample Tests

The concrete slabs were exposed to a hot air stream which simulated the exposure of a concrete pavement to the hot APU exhaust gases. Figure 5 shows the experimental set-up.

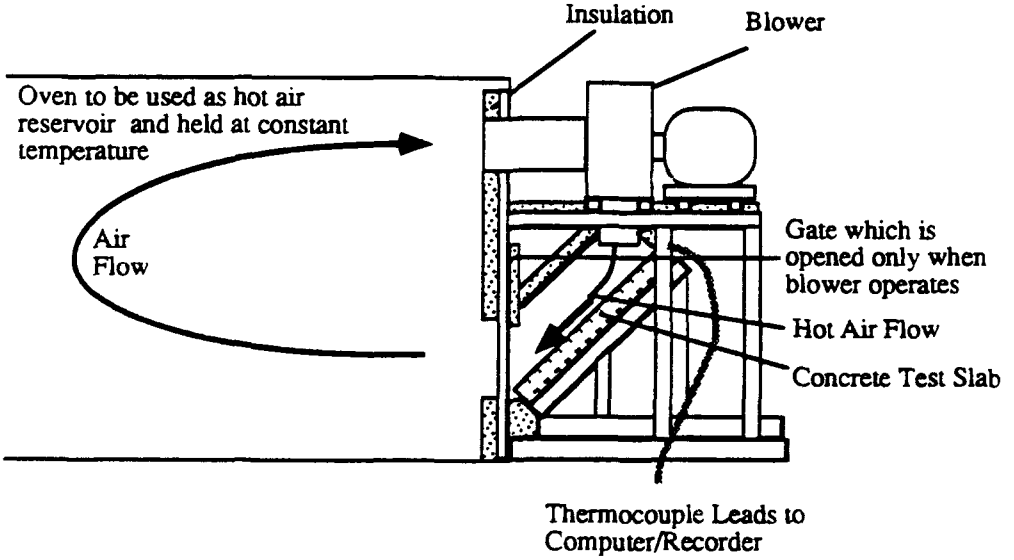

Figure 5. The Blower Unit

The blower directs hot air from the oven onto the surface of the slab at an angle of 45 degrees. The air flows over the slab and back into the oven. The slab was insulated in such a way that only its surface was exposed to the hot air. The surface was exposed for 30 minutes to the hot air, then the blower was shut off and the concrete slab pulled out of the unit to cool down. During heating and cooling the temperatures in the slab and the air stream were measured. The velocity of the air was also measured. The experiment was done at oven temperatures of 300F for the first three cycles and 400F for the next three cycles for each slab.

Before and after the heat cycles, the 'surface permeability' was measured. The set-up was as shown in Figure 6. A steel bell was sealed to the concrete surface and vacuum of 30 in Hg (~760 mm) applied for 7 minutes. The vacuum pump was disconnected and the pressure inside the bell increased due to the air flowing inside the bell through the concrete. The rate of pressure increase was measured in mm Hg per second, and represents a measure of the concrete surface quality (permeability). A similar set-up to estimate concrete surface durability after curing has been used and described in (11).

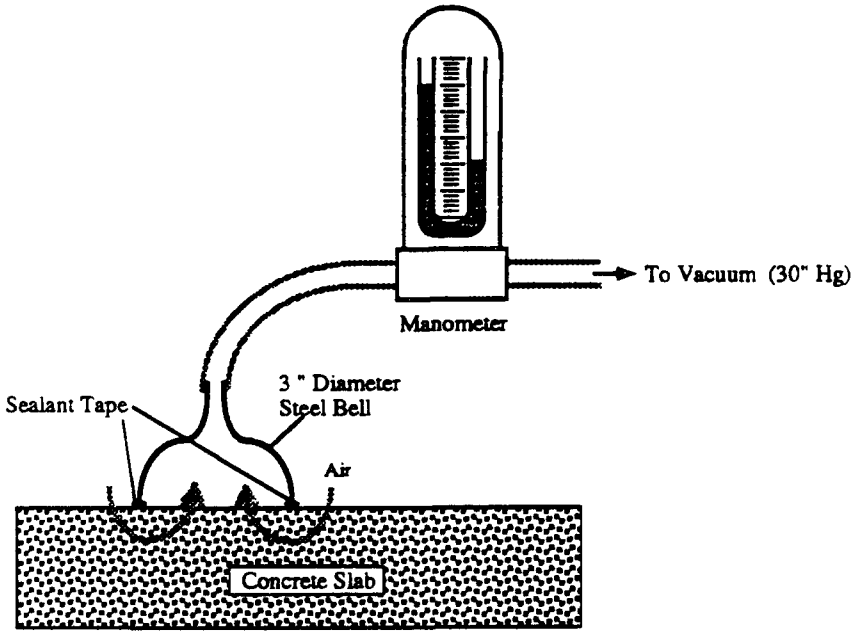

Figure 6. 'Surface Permeability' Measurements

Finite Element Models (FEM)

Analytical modeling of the effects of heat exposure to concrete pavements was conducted by Professor Peter Chang

of the University of Maryland. The modeling work consists of three parts:

- calculation of temperature distributions in the concrete from convective and conductive heating.
- calculation of stress contour plots for a monolithic material using transient heating.
- calculation of stresses at the interface, in the aggregate and in the matrix surrounding an aggregate for a simple model.

The temperature distributions have been calculated assuming an air flow parallel to the surface at 60 mph and 380F. The convection calculation was uncoupled from the conduction calculations. Further assumptions were a turbulent flow and concrete properties similar to those of high density metal filled Chemically Bonded Ceramics (CBC).

The stress calculations were made for a monolithic material used with average mechanical and heat properties for quartz and limestone concrete. Strengths, moduli of elasticity, heat capacity and heat conductivity do not vary much for the different concretes. The main difference between quartz and limestone concrete is their CTE due to the different CTE's of the aggregates. CTE's of $3*10^{-6}$ /F for limestone and $7*10^{-6}$ /F for quartz concrete were chosen (18).

Some of the calculation took shrinkage into account. The shrinkage of the mortar matrices as function of temperature were obtained from the dilatometer experiments.

The calculations of stresses in an interface and the adjacent aggregate and mortar were performed for a simple model of a spherical aggregate 1/2" below the surface as shown in Figure 7.

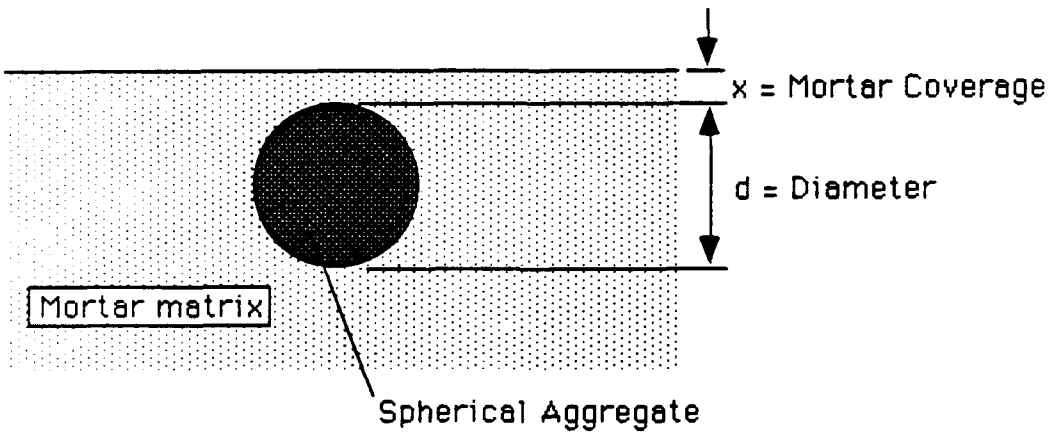

Figure 7. Model to Evaluate the Aggregate-Mortar Interface

Results

Mortar Experiments

Mechanical Properties

The flexural and compressive strengths for the mortar series are given as a function of the number of heat cycles in Figures 8 and 9, respectively.

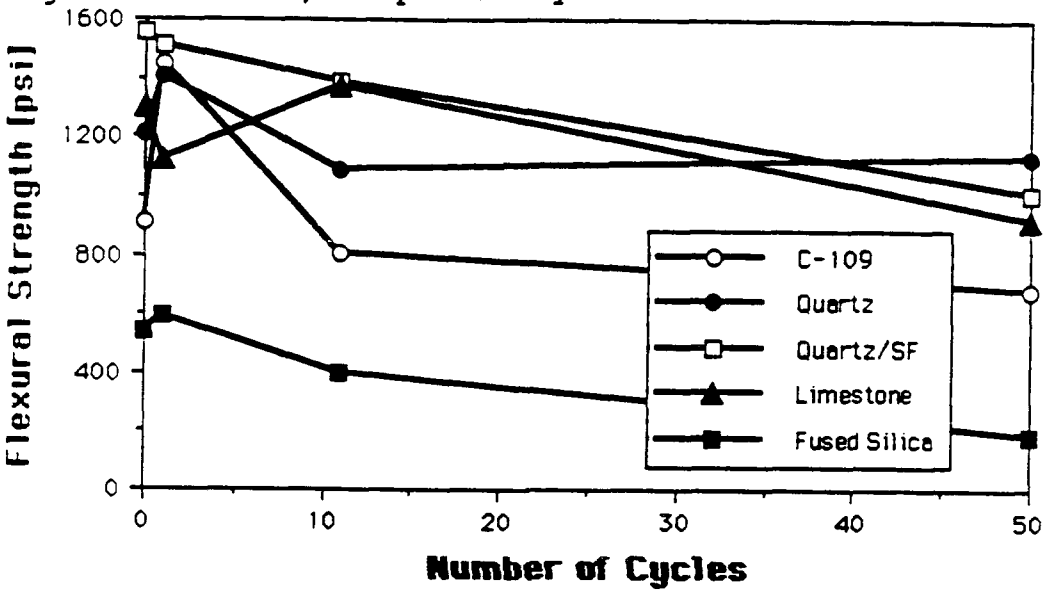

Figure 8. Flexural Strength Development with Heat Cycling

With the exception of the fused silica mortar all samples performed well and showed initial flexural strength well above the minimum requirement of 650 psi for pavements. Even after 50 cycles most of the flexural strengths values lie around 1,000 psi - still an excellent performance. But, the strength is definitely degrading with increasing heat cycles.

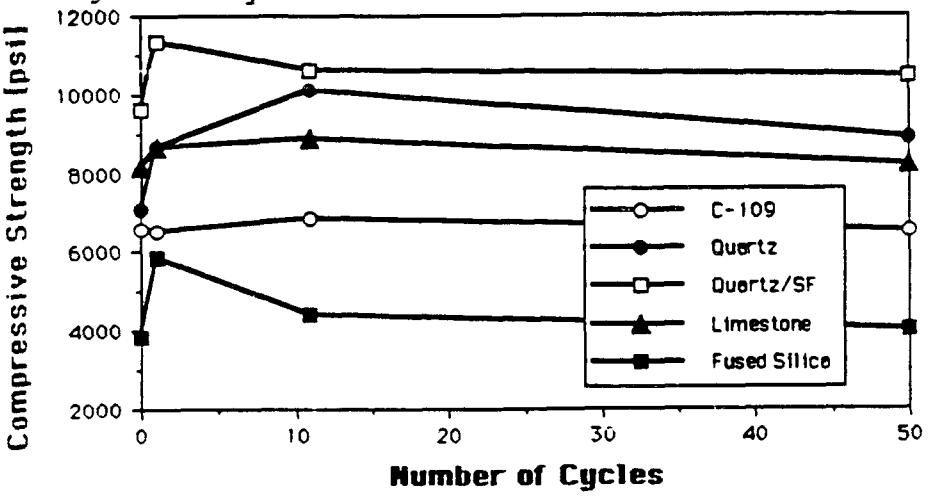

Figure 9. Compressive Strength Development with Heat Cycling

All the compressive strengths go up for the first 11 cycles, then start to go slowly down. Again, the fused silica mortar shows the less favorable behavior. The other mortars exhibit compressive strengths between 6,000 and 11,000 psi and can therefore be considered as high strength mortars according to the ACI.

Shrinkage

Shrinkage data are available from the expansion bar measurements as a function of heat cycles and from the dilatometer experiments. Shrinkages determined from the dilatometer measurements are given in Table IV for the five mortar series in different temperature ranges.

TABLE IV. Shrinkages for Mortars from Dilatometer Experiments

Temp. Range [F]	C-109	Quartz	Quartz/SF	Limestone	Fused Silica
77-131	.014	.016	.018	.015	.012
77-185	.022	.024	.035	.021	.026
77-239	.061	.042	.068	.038	.058
77-293	.094	.076	.117	.063	.109
77-347	.103	.100	.148	.090	.141
77-400	.107	.110	.171	.122	.164

All shrinkages are cumulative shrinkages given in percent. Shrinkages measured on the expansion bars are given in Figure 10 and compared to the total shrinkage at 400F from the dilatometer experiments.

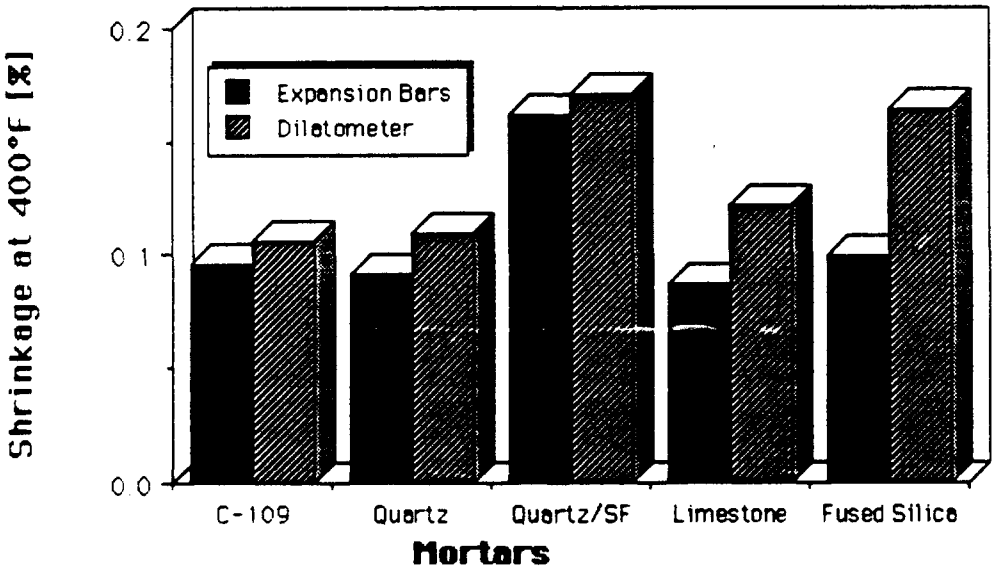

Figure 10. Shrinkage at 400F for the Mortar Series

From Table IV and the bar diagram, it is obvious that the quartz/SF mortar and the fused silica mortar show the highest shrinkage values. The shrinkages measured on expansion bars show lower values than those from dilatometer experiments. A possible explanation is the influence of moisture pick-up on shrinkage. Samples in the dilatometer do not pick-up moisture upon cooling, since they are in a closed environment. The expansion bars cool in the laboratory environment and easily pick-up moisture which leads to swelling.

This effect can be seen in Figure 11 where the shrinkage is plotted versus the weight change of the samples for the C-109 and quartz mortar. The different shrinkages and weights were measured for expansion bars after extended exposure to the humidity of the laboratory air. There is a strong relationship between the shrinkage and the weight loss of samples.

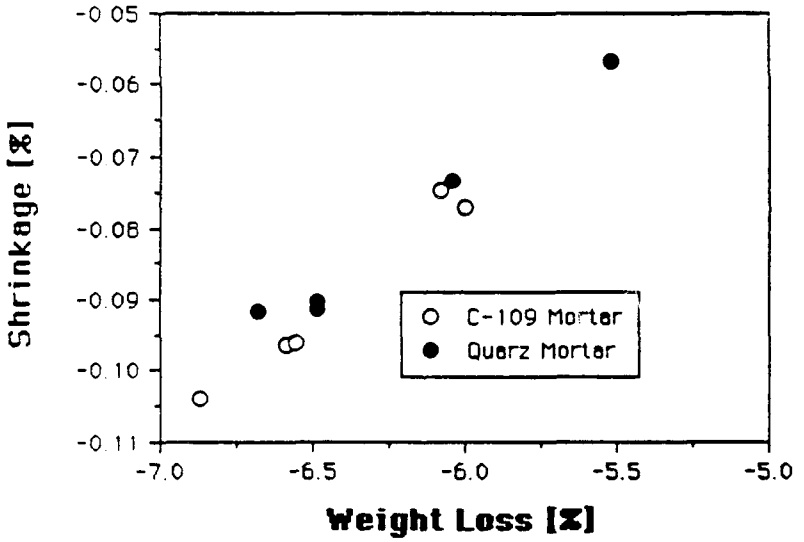

Figure 11. Shrinkage as a Function of Weight Loss

Coefficients of Thermal Expansion

The CTE's for the mortars in a temperature range of 77F to 400F are given in Table V.

Table V. CTE's for the Mortar Series*

C-109	Quartz	Quartz/SF	Limestone	Fused Silica
5.8915	5.8598	5.7700	3.1896	0.0866

*NOTE: Multiply all values by 10^{-6}/F.

The first three series with quartzitic aggregates exhibit CTE's around 5.8 to 5.9 $*10^{-6}$ /F, the limestone mortar is about half of that, and the use of fused silica as an aggregate reduces the coefficient of thermal expansion by two orders of magnitude.

MIP

The measurements of pore size distribution with mercury intrusion porosimetry resulted for all mortars in a type of curve as shown in Figure 12.

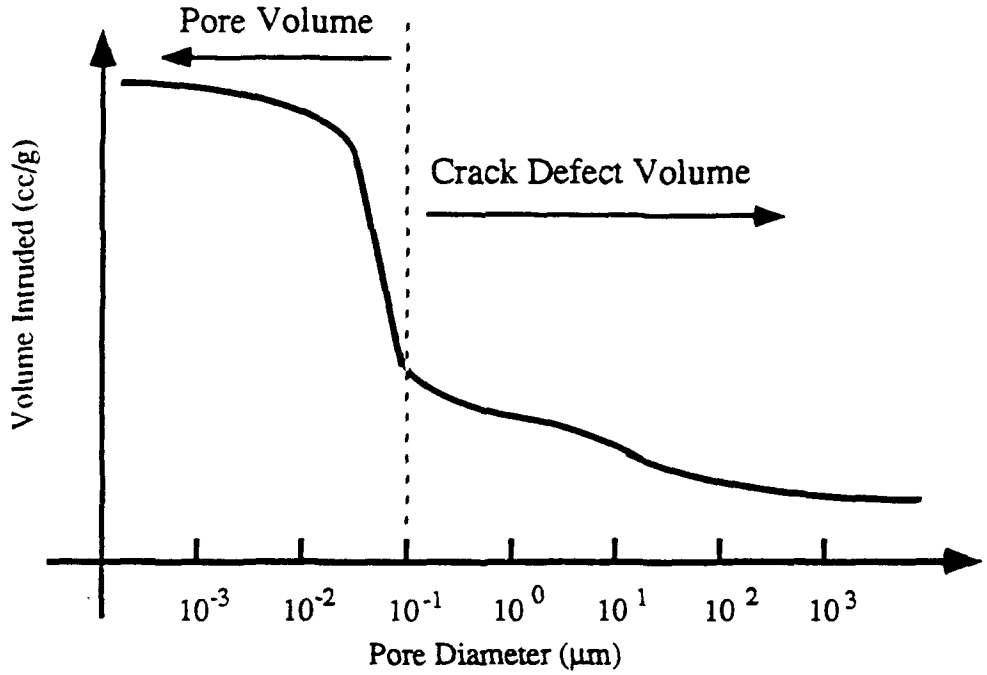

Figure 12. Basic Behavior of the Cumulative Intrusion Volume for the Mortars

The intruded volume of mercury is displayed as a function of the pore diameter. The curve can be divided into two sections. The first starts at diameters of about 300 um ($1.181*10^{-2}$ in.) and goes down to about 0.2 um ($7.874*10^{-6}$ in.). The second part starts around 0.2 um ($7.874*10^{-6}$ in.) and shows a steep increase of the intruded volume, levels off at about 0.02 um ($7.874*10^{-7}$ in.) and goes down to about 0.002 um ($7.874*10^{-8}$ in.). This second part represents the capillary and the coarse part of the gel pore system in a cementitious material. The first

section of the curve reflects the volume of defects and cracks.

Figures 13 through 17 show these MIP curves for the five mortars after different numbers of heat cycles. Although there are differences, the various materials show the same pattern:

- the second part of the curve, representing the pore volumes is not very much affected by the heat cycles.
- the first part of the curve - the crack or defect volume - increases with increasing heat cycles.

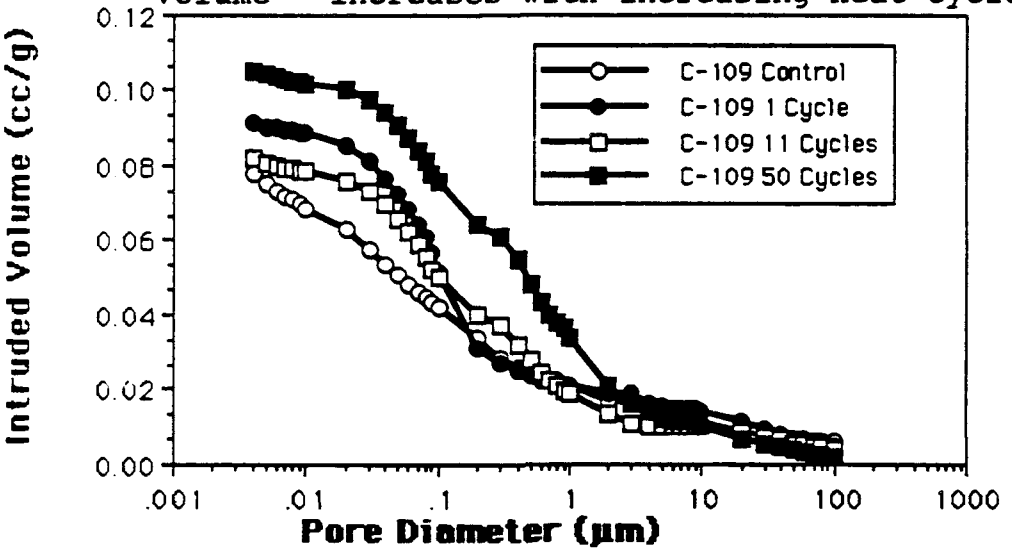

Figure 13. MIP Curves for C-109 Mortar

The C-109 mortar shows a constant increase in cracks starting with the first cycle and resulting in a crack volume of about 0.006 cc/g after 50 heat cycles.

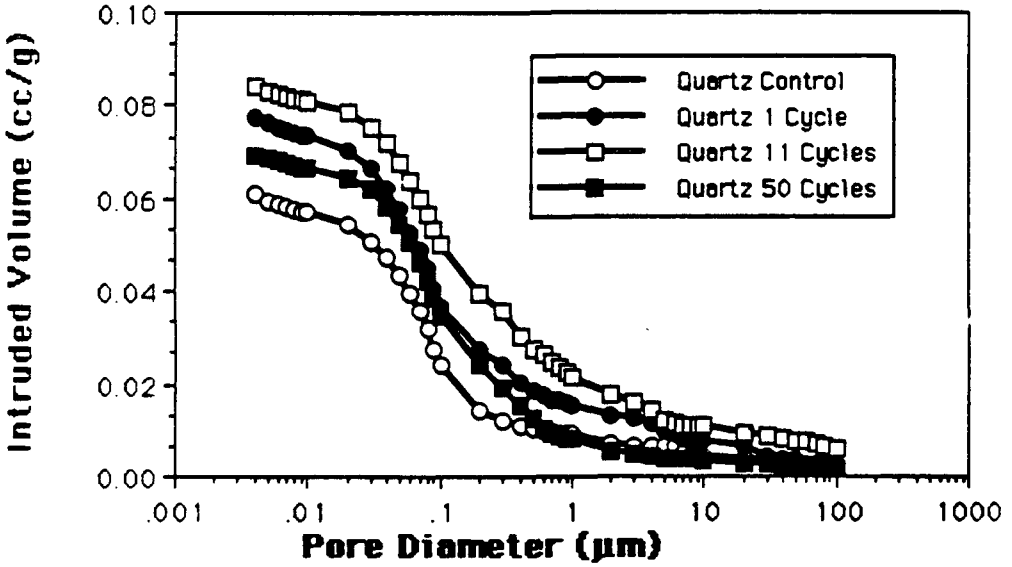

Figure 14. MIP Curves for Quartz Mortar

The quartz mortar shows this behavior up to 11 cycles. After 50 cycles, however, the crack volume decreased.

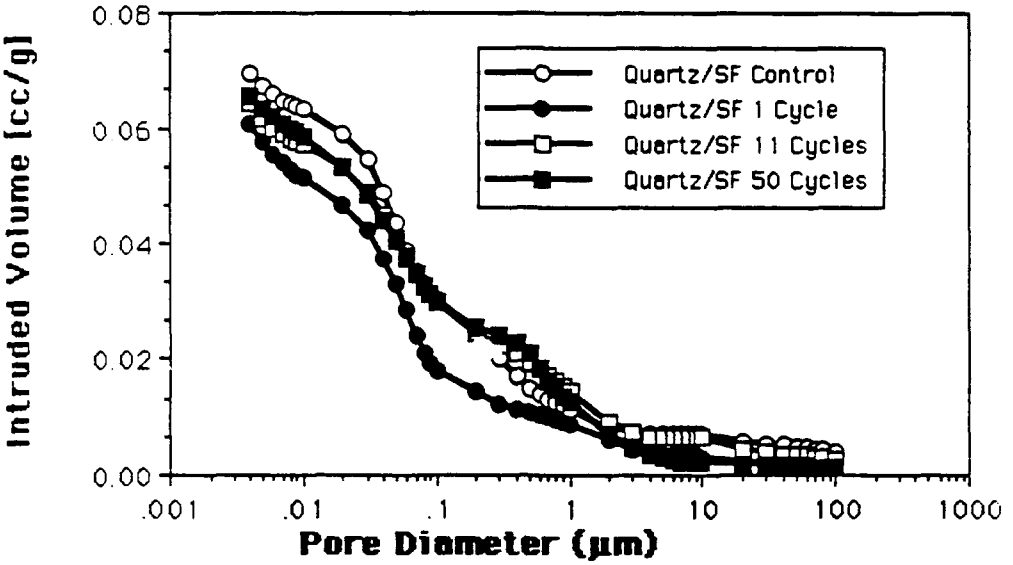

Figure 15. MIP Curves for Quartz/SF Mortar

The quartz/SF mortar shows a pronounced densification of the defect/crack volume after 1 cycle. This might be due to the reactivity of the silica fume at high temperatures as long as moisture is present. After 11 and 50 cycles the crack volume increases and is higher than the one measured for the control sample. For these samples, moisture was no longer present.

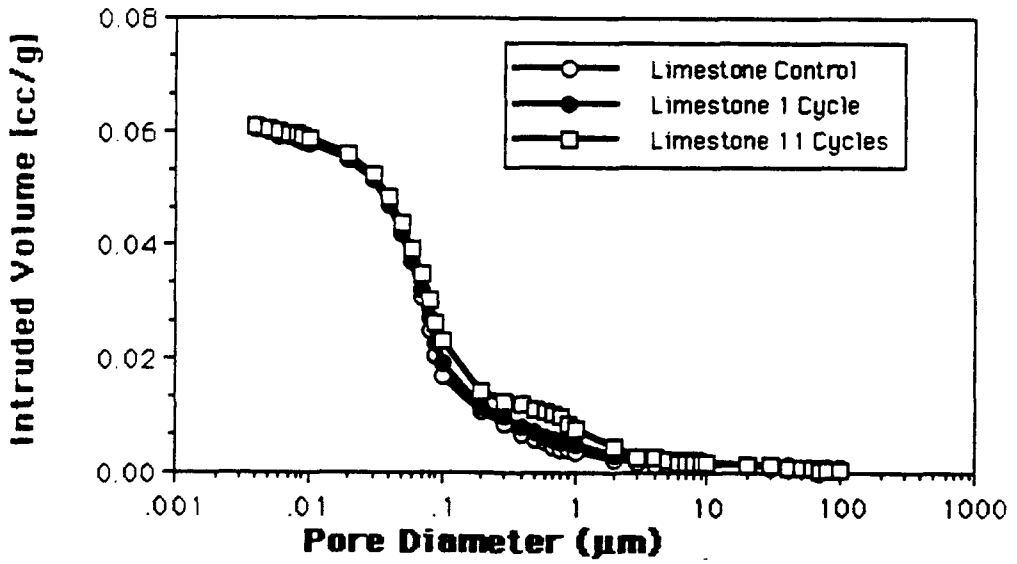

Figure 16. MIP Curves for Limestone Mortar

The limestone mortar shows almost no difference after 1 cycle. Crack volume is slightly increased after 11 cycles.

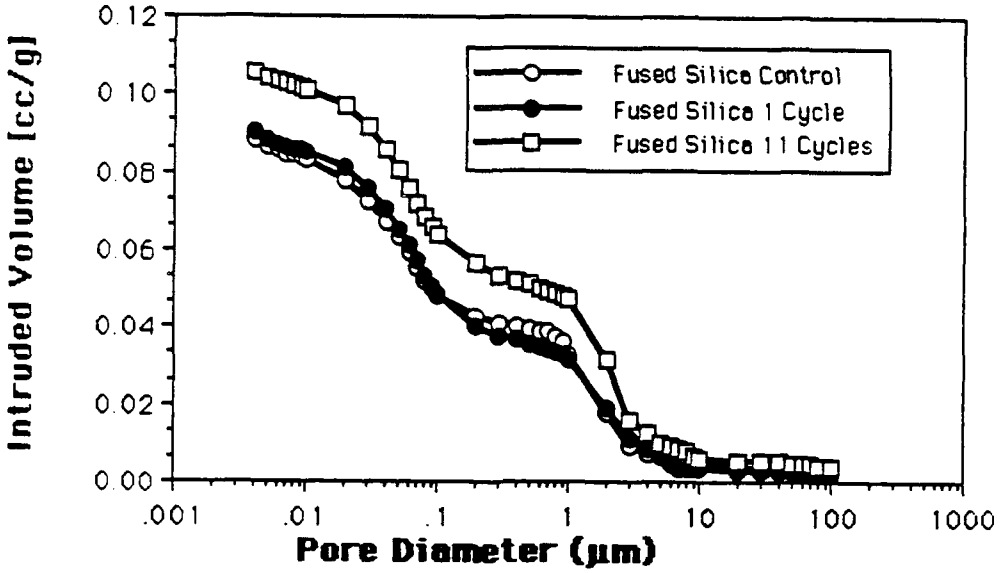

Figure 17. MIP Curves for Fused Silica Mortar

The fused silica mortar has almost identical structures for the control sample and after 1 heat cycle - the crack volume is slightly reduced. After 11 cycles, however, this material shows the most dramatic increase in cracking.

Figure 18 shows a comparison of the different mortars after 11 cycles of heat exposure.

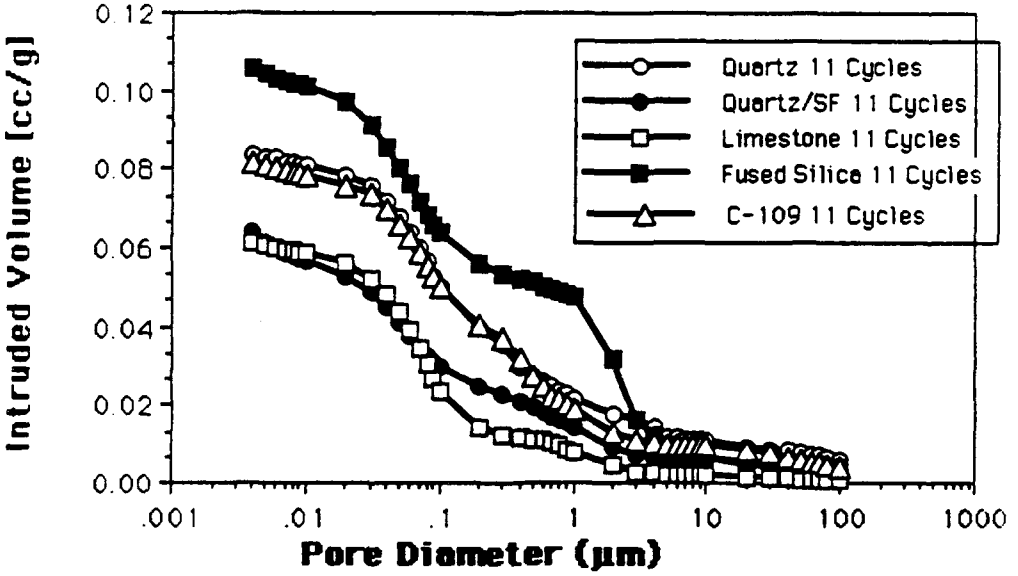

Figure 18. Comparison of MIP Curves for the Different Mortars After 11 Heat Cycles

The limestone mortar shows the lowest defect volume, followed by the quartz/SF mortar. The quartz and C-109 mortars are very similar but higher in defects than the limestone and quartz/SF mortars. The fused silica shows by far the highest volume of cracks.

Concrete Experiments

Temperature Profiles

Figures 19 through 22 show the temperature as a function of time at different locations of the quartz concrete slab during a 300F and 400F heat cycle, respectively.* Corresponding diagrams for limestone and quartz/SF concretes are given in appendix A1 through A8.

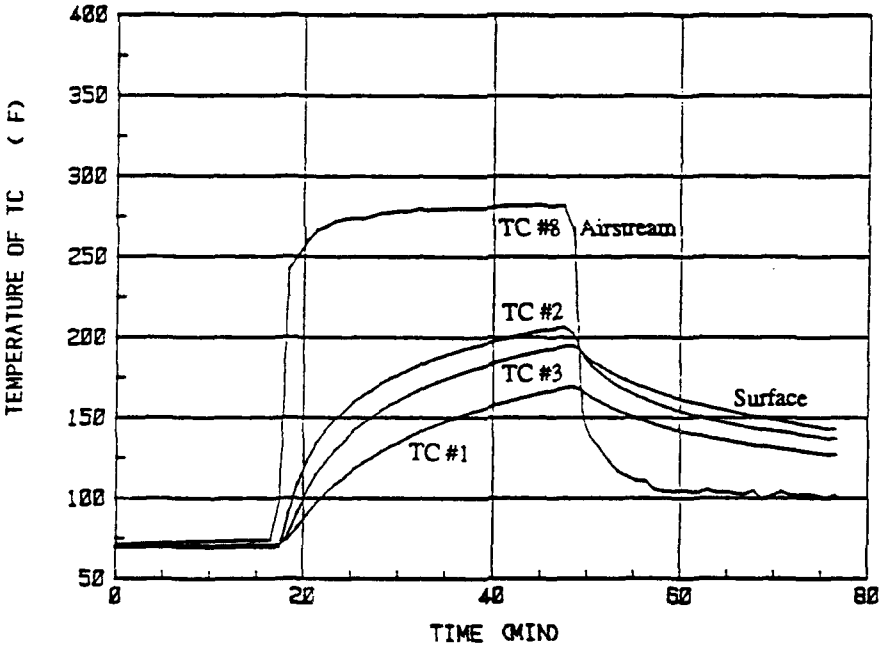

Figure 19. Surface Temperatures of Concrete During a 30 Minute 300F Air Stream Exposure

*NOTE: The oven/blower system used in the exposure tests did not provide gas flow conditions that closely modeled F/A-18 exhaust parameters.

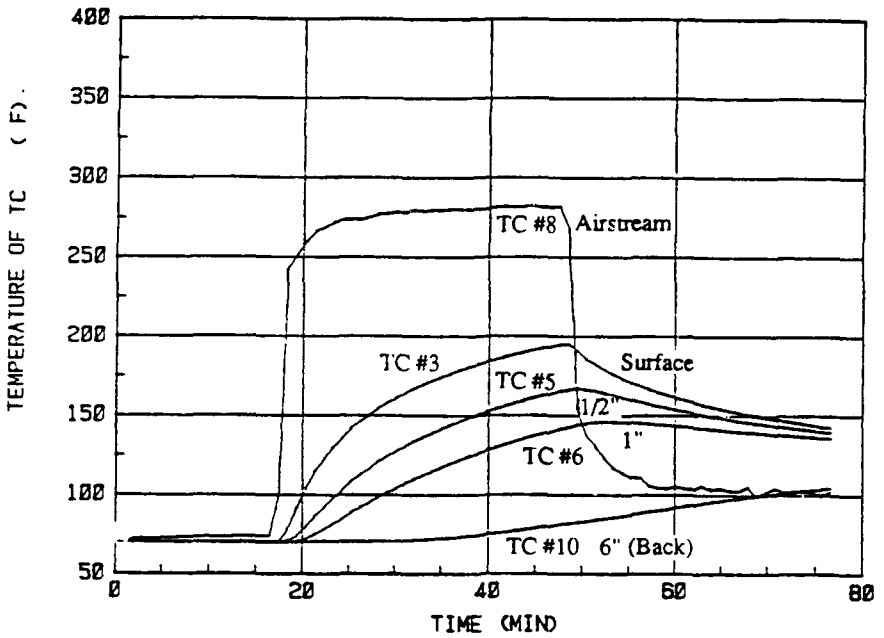

Figure 20. Temperatures at the Surface and at Various Depths at the Impingement Area for a 300F Heat Cycle

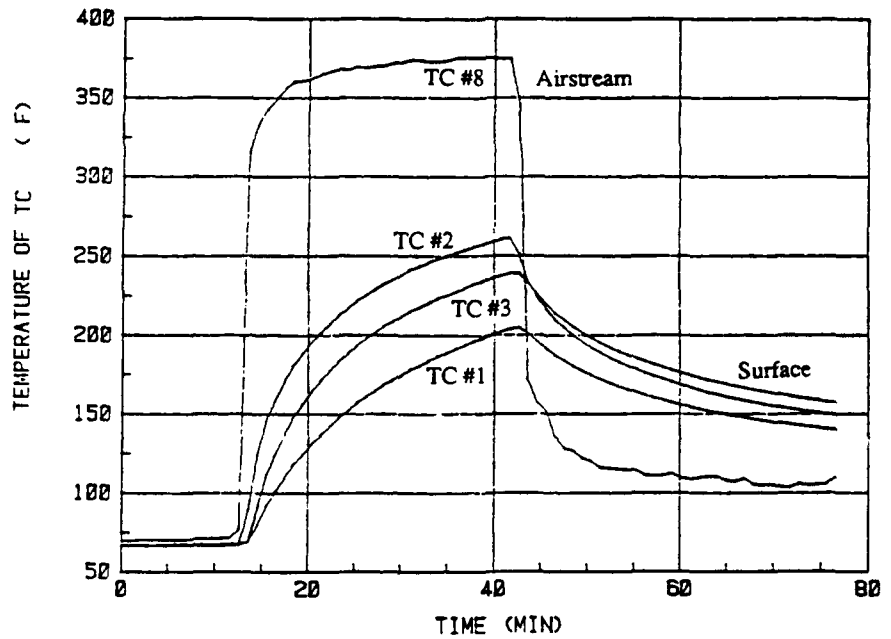

Figure 21. Surface Temperatures of Concrete During a 400F Heat Cycle

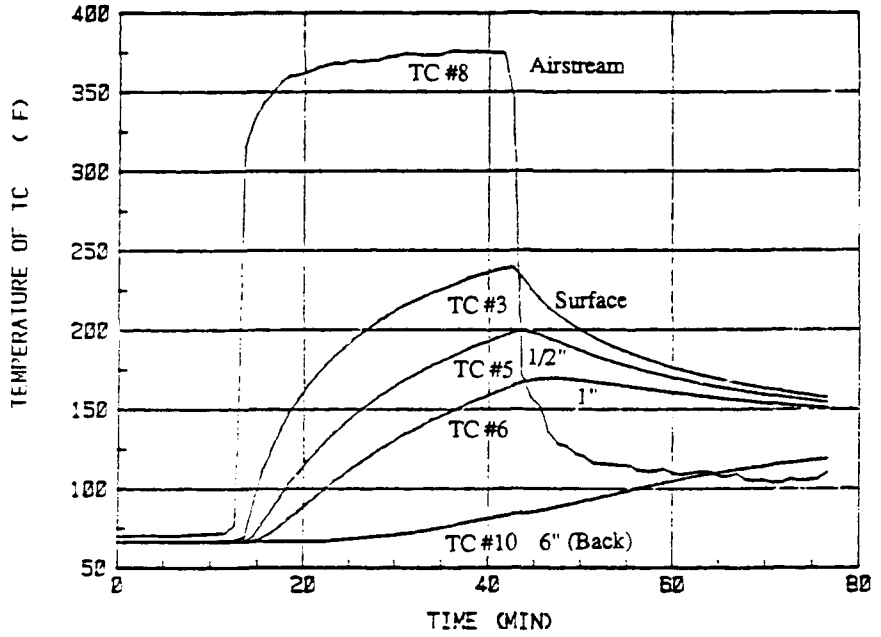

Figure 22. Temperature at the Surface and at Various Depths at the Impingement Area During a 400F Heat Cycle

Thermocouple #8 represents for all plots the air stream temperature about 1/2" above the surface in the middle of the concrete slab. Air speeds measured at that location were around 70-80 mph. The temperatures reached were about 275F and 375F for initial oven temperatures of 300F and 400F.

The maximum surface temperatures (thermocouples 1 through 3) range between 160F and 220F after 30 minutes of hot air exposure during a 300F cycle and between 200F and 280F for a 400F exposure. This holds true for all samples measured. The variation is caused by the different locations of the thermocouples and by slightly different concrete covers above them. The higher temperatures are generally measured in the area of impingement.

Temperatures at depths of 1/2 inch range from 170 to 180F (300F cycle) and 200 to 230F (400F cycle) for all concretes. One inch below the surface these numbers are 140 to 155F and 160 to 180F, respectively. The variations of temperature for different slabs are much less pronounced inside than on the surface or slightly below the surface of the concretes.

The temperatures on the back side of the specimen (6" from the surface) reach their maximum of 100 to 120F about 30 minutes after the blower has been shut off (one hour after start of test).

Surface Permeability

The quality of the concrete surface due to heat cycling is shown in Figures 23 and 24 in terms of the vacuum decay. In these Figures, cycles 1 through 3 were at 300F and cycles 4 through 6 at 400F. With an increasing number of heat cycles the vacuum in the steel bell degrades quicker indicating that air is flowing more rapidly through the concrete.

Looking at the absolute numbers in Figure 23, the limestone and quartz/SF concrete perform much better with both curves lying under the curve for the quartz concrete. These two samples showed a much denser concrete initially.

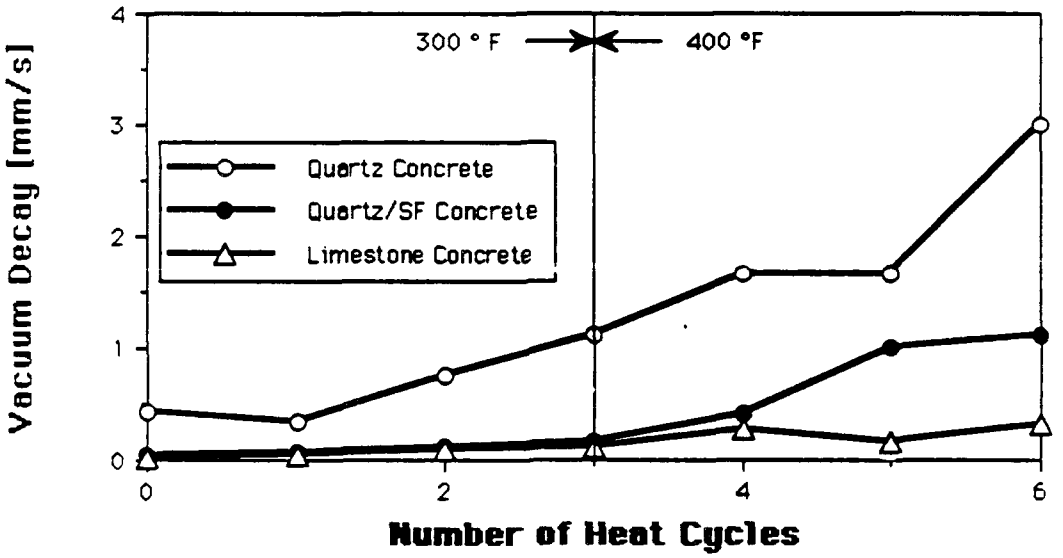

Figure 23. Vacuum decay Versus Number of Heat Cycles in the Area of Impingment

The rate of surface degradation, which is expressed as the relative vacuum decay in Figure 24, however, is higher for the limestone and the quartz/SF concretes, especially after the exposure to the 400F heat cycles. The apparently better performance of the limestone concrete after 5 cycles was caused by moisture pick-up between the cool down phase and the measurement (5 days).

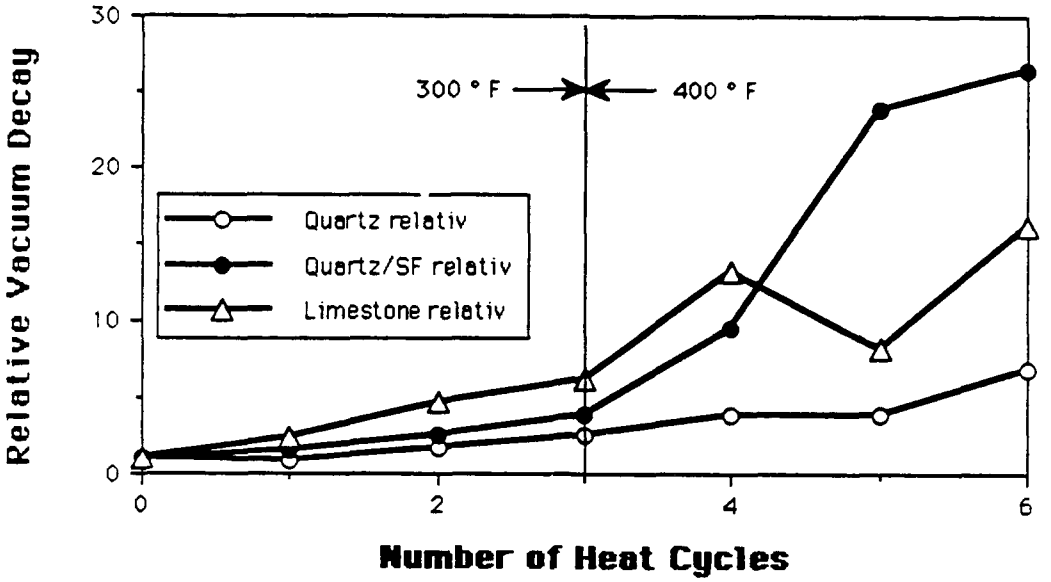

Figure 24. Relative Vacuum Decay for the Same Area as in Figure 23

Modeling

Temperature Distribution

Modeled and measured temperature distributions are shown in Figure 25. The measured temperatures were from F/A-18 APU exhaust footprint tests conducted by the Naval Air Propulsion Center on a concrete slab (aggregate composition not determined).

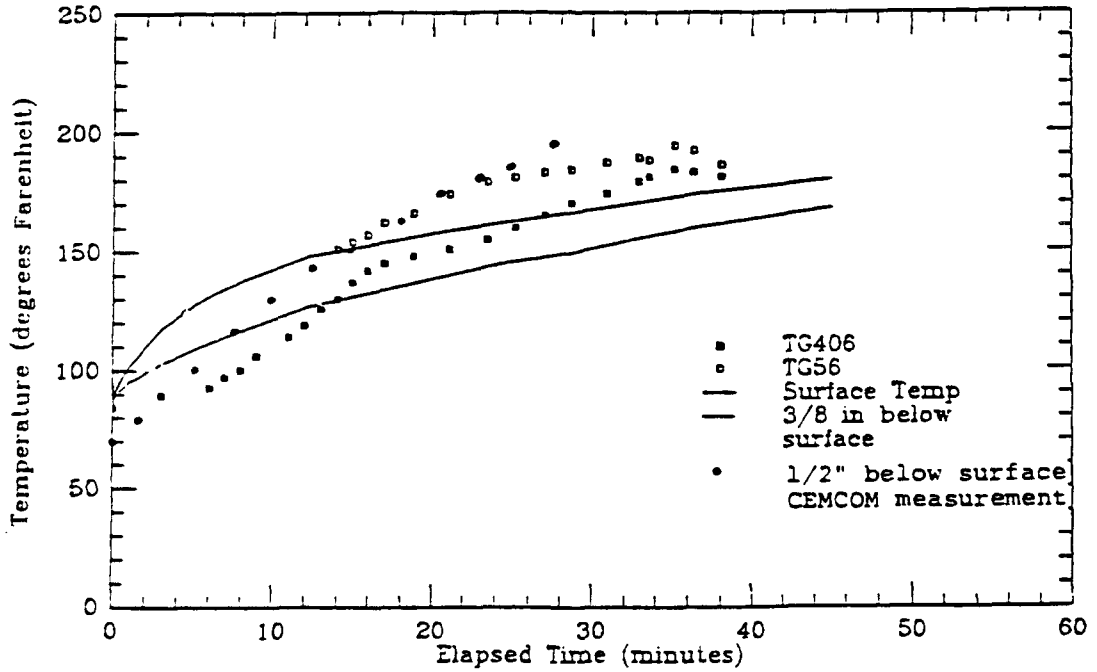

Figure 25. Comparison of Experimental and Theoretical Temperature Profiles

The data measured at a 1/2 inch depth of the concrete slab compare very well with the 'TG56' set measured at 3/8" taking into account that the variation in temperature at that depth is around ±15F. The modeled curve, however, is definitely below the experimentally obtained. This is probably due to the assumptions listed in the modeling paragraph earlier in this report. The two major differences in the assumptions as compared to the experiment are:

- a flow parallel to the surface as opposed to a 45 degree impingement.
- the use of dense, metal filled CBC properties which would explain a slower heat up rate than ordinary concrete.

Stress Contours

The original data and diagrams as provided by Professor Chang are in appendix A9 - A23. Some black and white copies are displayed in Figures 26 and 27. The figures show stresses in a quartz/SF concrete at the end of a 30 minute heating phase. Calculations have been made taking shrinkage into account and using only the shrinkage occurring after the cool down phase.

Calculations without shrinkage are given in appendix A9 and A12. The plot in A12 (stress contours for a quartz concrete without shrinkage) also holds true for the quartz/SF concrete, because the silica fume affects only the shrinkage behavior of the concrete.

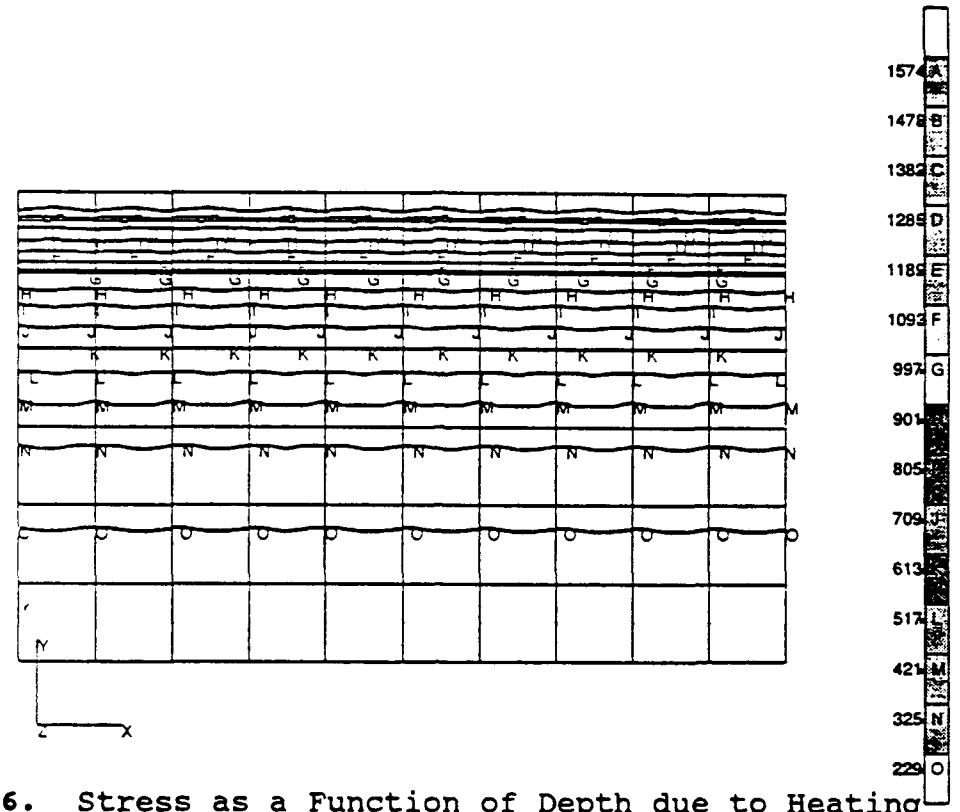

Figure 26. Stress as a Function of Depth due to Heating (Including Shrinkage)

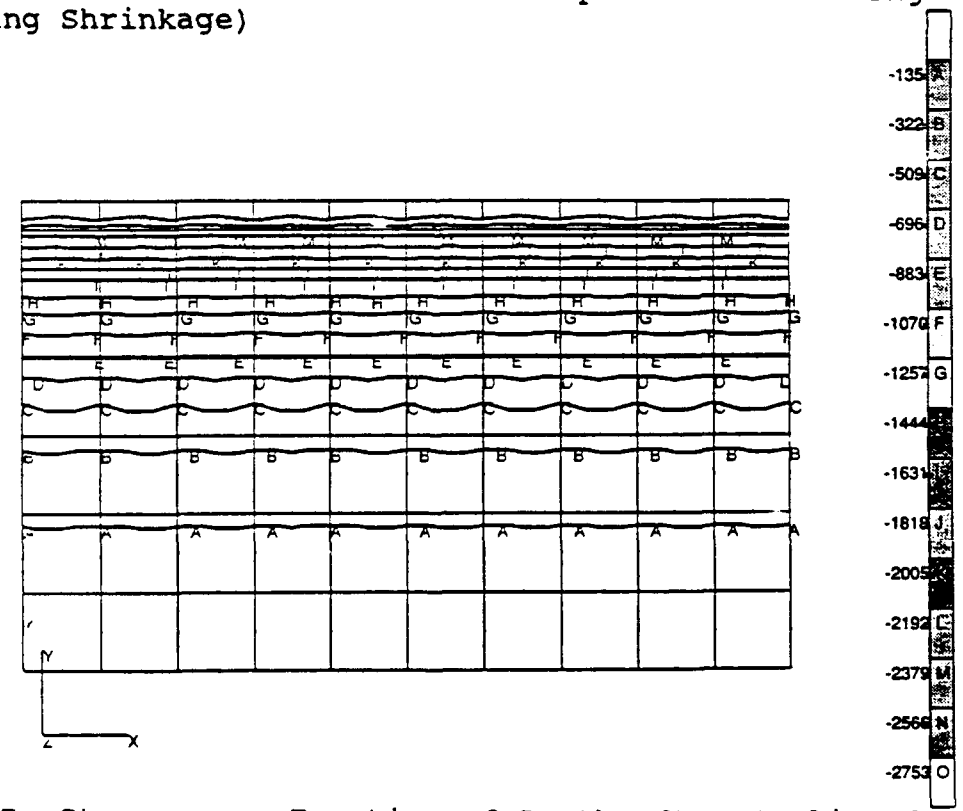

Figure 27. Stress as a Function of Depth After Cooling due to Shrinkage

Heating the concrete creates compressive stresses of up to 3000 psi due to the CTE of aggregates and matrix as shown in appendix A9 and A12. The limestone concrete shows lower stresses than the quartz and/or quartz/SF concrete. If the model allows the concrete to shrink (Figure 26 appendix A10 and A13) these compressive stresses are mitigated. This is due to the superposition of tensile stresses due to shrinkage of the matrix. This effect is most visible for the limestone concrete (compare A9 to A10). For the quartz and quartz/SF concrete the top layer of stresses becomes thinner. These tensile stresses, however, remain after cool down since the shrinkage is permanent. Figure 27 as well as appendix A11 and A14 shows those remaining tensile stresses. The magnitude of the stresses decreases in order from the quartz/SF followed by the quartz and finally by the limestone concrete. This corresponds to a decrease in shrinkage in the temperature range up to 200F (see Table IV). It should be noted that the compressive stresses created during heating are well below the compressive strength of the material. The permanent tensile stresses, however, can exceed the tensile stress capability of the concrete, especially in the case of the quartz/SF concrete.

Stresses for the Interface

Appendix A17-A20 show the net and blow-ups thereof used to calculate strains and stresses for the interface model. Appendix A21-A23 show first and second principal stresses in matrix and aggregate for a limestone matrix-limestone aggregate (3/4") combination after 30 minutes of heating. Shrinkage is not included in the calculation. Spring forces and stresses thereof are given in Table VI. Negative values are compressive; positive numbers are tensile stresses. The location of the spring elements in the interface is shown in appendix A20. Element #51 through 63 are radial forces, elements #64-76 represent tangential forces and stresses respectively.

Table VI. Spring Forces Between Matrix and Aggregate

Element #	Force (lbs.)	Stress (psi)
	radial	
51	7.86	80.2
52	15.96	162.9
53	-10.99	-112.1
54	-65.34	-666.7
55	-58.78	-599.8
56	-132.60	-1353.1
57	-72.98	-744.7
58	-115.80	-1181.6
59	-43.70	-445.9
60	-42.59	-434.6
61	-3.71	-37.9
62	-15.42	-157.3
63	-6.83	-69.7
	tangential	
64	0	0
65	-50.07	-510.9
66	-45.16	-460.8
67	-96.16	-981.2
68	-40.66	-414.9
69	-42.52	-433.9
70	-3.66	-37.3
71	-38.96	-397.6
72	-35.85	-365.8
73	-72.35	-738.3
74	-30.28	-309.0
75	-32.66	-333.3
76	0	0

The stresses created at the interface reach a maximum of up to 1350 psi. These stresses put the aggregate into compression - it assumes a more oval-like shape. The influence of shrinkage or other combinations of aggregate and matrix are difficult to predict from the calculations made so far.

Discussion

The results presented so far were obtained for mortars and concrete made in a laboratory environment with a water cement ratio of 0.40 and cured under optimum conditions. This resulted in a very good performance of the materials, with the exception of the fused silica mortar. The mechanical properties classify these materials as high strength concretes. The flexural strength were up to over two times higher than required for Navy pavements.

Complete failure of an airfield pavement typically does not occur for 1 - 2 years during which time the material is subjected to hundreds of heating cycles. The relatively short time period for this project did not allow observation of the phenomena directly. Therefore, the program was designed to look at the changes that precede failure which are pore structure coarsening, increasing permeability and degradation of mechanical properties with thermal cycling.

Even though no total failure has occurred yet, a working hypothesis can be developed from these results. The degradation of the microstructure and the mechanical properties is caused by the microcracking of the cement paste and the mortar matrix, respectively. The source of this microcracking is believed to be due primarily to drying shrinkage. This hypothesis provides and explains the mechanism that leads to failure, how the failure develops and what mix design parameters of a concrete are prone to a fatigue failure when exposed to heating. The hypothesis has to be proved in further long term and field studies before recommendations can be made on how to design a heat resistant airfield pavement.

The microcracking mechanism which leads to a fatigue failure has also been observed for concrete subjected to relatively high loads for long periods of time. Microcracking starts to develop when concrete is heated (mismatch in CTE) and/or drying (shrinkage). The formation and propagation of cracks in concrete due to heating and cooling has been observed by other researchers using acoustic emission (7). It also was observed using MIP on heated samples as well as on mechanically loaded samples (13). In our study it could be seen by an increase in a pore volume which is associated with the creation and growing of cracks. The intruded volume curves show these cracks very clearly as a second peak - the distribution is bimodal. The size of cracks between 1 um and .1 um corresponds to crack sizes measured on concrete samples subjected to the same temperatures (13).

Along with an increase in microcracking, the flexural strength of specimens went down. Flexural strength is most sensitive to cracks which can be considered notches. For the concrete slabs in our study, microcracking resulted in an increased surface permeability. The cracks render the surface more porous allowing more air to flow through it.

Eventually the increase of microcracking leads to a failure. In a standard mechanical test, the same mechanisms happens. a network of microcracks is created at relatively low loads (~20% of the ultimate load) and keeps growing until the sample fails. For a fatigue failure, the

microcrack network also grows until failure of the whole sample occurs. It takes, however, much more time.

The modeling work shows (stress contour plots) that cracking most likely happens on cool down of concrete, when the originally compressive stresses are overcome by tensile stresses. The fact that most damage to concrete is done during the cooling phase has been suggested by other researchers (7,14),including those cited by the Navy (15). The tensile stresses depend largely on the shrinkage associated with the drying of the samples. This goes along with the experimental results. The fused silica mortar which showed a high shrinkage, also exhibits the worst strength performance and shows the highest crack volume. Originally, the fused silica had been chosen for its low CTE. The mortar's CTE was two orders of magnitude lower than that of quartz or limestone samples and therefore would have very low thermal stresses if considered as a monolithic material. The difference in CTE between the fused silica sand and the cement paste matrix, however, is very high which would induce high stresses at the interface leading to debonding. The cracks observed most likely are caused by debonding due to high shrinkage and a large difference in CTE's.

Silica fume concrete, though originally with high strength and low permeability, showed the fastest increase in surface permeability and a decrease in flexural strength beyond 11 cycles for the mortars. The mismatch between sand and cement paste CTE was not very high - in fact the quartzitic sand comes the closest to the paste's CTE. This indicates that the shrinkage, which was high for the silica fume modified matrix is indeed a major player in causing a heat fatigue failure.

The performance of the quartz and C-109 mortar, as determined by flexural strength, were better during the cyclic thermal loading. They performed better not in terms of absolute strength values but by showing no further decrease in flexural strength between 11 and 50 heat cycles. This might be due to a moderate shrinkage and a close match of the CTE's of cement paste matrix and quartz sand. This match is also recommended in the Military Handbook for 'Rigid Pavement Design for Airfields' (16) where the use of sand and aggregates from the same material is specified (matrix-aggregate match).

The other samples, though performing very well in the beginning, show a continued downward trend. This continued trend would lead to a failure of the pavement after a sufficient number of cycles.

Another factor not fully investigated here is a very realistic moist-dry cycling. When concrete is heated it dries and shrinks. After cool down it reabsorbs moisture and swells. This effect which relates shrinkage and swelling to moisture loss and gain could be clearly seen in this study. This cyclic loading most probably would favor a faster failure than pure heat cycles without moisture pick-up in between.

As described in the preceding paragraphs, a mechanism which explains a scaling of concrete surfaces due to thermal cycling has been found and could be experimentally shown to happen in concrete. The samples tested showed an increasing degradation with increasing number of heat cycles, however, never failed totally as observed for the apron parking areas. This is due to the fact, that the limited time did not allow to expose the samples to a sufficient number of heat cycles. Furthermore, the samples showed very good mechanical properties so that a failure might occur after even more cycles than observed in the field. The degradation of a concrete surface could be observed by a non-destructive permeability measurement - a method which might be applied to airfield pavements to detect developing damages that can be repaired easily and inexpensively.

Conclusions

The results presented and discussed in the preceding sections provided a basis of understanding the fatigue failure of concrete pavements subject to the hot exhaust gases from an APU. They allow to draw the following conclusions:

1. Concrete and mortar exposed to one cycle of thermal treatment up to 400F initially gains flexural and compressive strength.
2. Continuing heat cycling result in strength loss.
3. The strength loss up to 50 cycles was minimized for mortars containing quartzitic aggregates and no additives.
4. The heat cycling also leads to a degradation (coarsening of the pore structure) of the surface of a concrete even though the surface visibly looks intact.
5. The decrease in concrete performance is caused by microcracking affected by the CTE mismatch of aggregate and matrix and more important by the shrinkage of the matrix.
6. The microcracking and its increase with increasing cycles could be shown by MIP.

7. The modeling work confirmed experimental results by demonstrating that compressive stresses produced during a heating cycle due to CTE mismatch become tensile in the cool down phase due to the shrinkage.

Outlook: Future Research and Suggestions

The results obtained in Phase I of this project provide an excellent basis to start to understand the mechanisms and properties of concrete responsible for its heat fatigue failure. The continuation should focus on three areas:

- a broadening of the basic knowledge, especially where the effect of moisture is concerned.
- continuation of the modeling work.
- design and evaluation of heat resistant pavements including novel techniques.

Future Research

During the investigation it became apparent that not only the temperature exposure but also moisture pick-up after cool down affect the dimensional stability of the concrete. This effect has to be looked into further. Shrinkage and swelling are caused by moisture diffusing in and out of a cementitious system. Experiments would look into a cycling program for mortars similar to the one carried out so far. In addition, a 24 hour moist exposure - 75% relative humidity (r. h.) - would be added between the heat cycles. For the concrete slabs spraying with water (rain) between cycles would be appropriate.

In addition, the concrete slabs manufactured so far will be subjected to more heat cycles. Also, concrete with lower quality but still within the specifications for pavements will be cast and tested. The influence of the maximum aggregate size will be investigated. The slabs tested so far - at least the quartz concrete - might already provide sufficient resistance to cyclic thermal loading.

The modeling work should continue with the calculations for the interface model. This model could be extended to a more complex representation of the composite concrete. Repeated heating, preferably with calculation of crack patterns should be a major objective.

Suggestions

Given the present state of knowledge, shrinkage is the major player in creating and growing microcracks. Attempts to design a heat resistant (thermal cycling) pavement have to concentrate to reduce or eliminate shrinkage. There are several ways which can be proposed:

- Reduce the water/cement ratio further. This would reduce the degree of hydration and therefore the amount of phases contributing to shrinkage. Furthermore the resulting concrete will exhibit a higher strength. Using superplasticizers will make the mixing and casting of such a concrete easy.

- Autoclave concrete which leads to the mineralization of phases. For this approach additional silicate phases have to be provided in the mix design. The resulting mineral phases are more stable than the semi-crystalline CSH phases in normal concrete and show much less shrinkage.

- Seal concrete after drying which prevents it from further moisture loss or gain. The movement of moisture in and out of a concrete basically causes shrinkage. If this process can be eliminated without affecting the concretes performance, the shrinkage should be largely reduced.

- Design a concrete with shrinkage compensating additives. This shrinkage compensation has to be stable at elevated temperatures and/or moisture up-take. It would be achieved by adding a well balanced amount of an expansive material in order to end up with a total shrinkage close to zero.

The applicability and effectiveness of these measures has to be proven not only in the laboratory but also in field experiments. This means pavements in apron parking areas where F/A-18's are stationed have to be cast with modified concretes. As those areas are being used they have to be monitored very closely.

Investigations to further build a sound understanding of fatigue failure and the work on modified concrete materials should make it very likely to come up with a heat resistant pavement design.

References

1. Schneider, U.; "Behavior of Concrete at High Temperatures", Deutscher Ausschuss fur Stahlbeton; Heft 337; Berlin, (1982).
2. Carette, G. G. and Malhotra, V. M.; "Performance of Dolostone and Limestone Concretes at Sustained High Temperatures"; American Society for Testing and Materials; Philadelphia; (1985); pp. 38-67.
3. Sullivan, P. J. and Poucher, M. P.; "The Influence of Temperature on the Physical Properties of Concrete and Mortar in the Range 20 C to 400 C".
4. Lankard, D. R., Birkimer, D. L., Fondriest, F. F., and Snyder, M. J.; "Effects of Moisture Content on the Structural Properties of Portland Cement Concrete Exposed to Temperatures up to 500F".
5. Diederichs, U., Jamppanen, U-M., Penttala, V.; "Behavior of High Strength Concrete at High Temperatures"; Espoo 1989.
6. Seeberger, J., Kropp, J. and Hilsdorf, H.; "Festigkeitsverhalten und Strukturanderungen von Beton bei Temperaturbeanspruchung bis 250C"; Deutscher Ausschuss fur Stahlbeton; Heft 360; Berlin (1985).
7. Kordina, K., Wydra, W. and Ehm, C.; "Analysis of the Developing Damage of Concrete due to Heating and Cooling"; 'Evaluation and Repair of Fire Damage to Concrete'; ACI Committee 216; pp. 87-114.
8. Odler, I. and Zurz, A.; "Structure and Bond Strength of Cement - Aggregate Interfaces"; 'Bonding in Cementitious Composites'; Materials Research Society Symposium; Dec. 4, 1987, Boston, Massachusetts; vol. 114; pp. 21-28.
9. Zhi Yuan, C. and Jian Guo, W.; "Effect of Bond Strength Between Aggregate and Cement Paste on the Mechanical Behavior of Concrete"; 'Bonding in Cementitious Composites'; Materials Research Society Symposium; Dec. 4, 1987; Boston, Massachusetts; vol. 114; pp. 41-48.
10. Drake, L.C.; "Pore-Size Distributions in Porous Materials - Application of High Pressure Mercury Porosimeter to Cracking Catalysts"; 'Industrial and Engineering Chemistry'; 41; No. 4; (1949).
11. Schonlin, K. and Hilsdorf, H. K.; "Permeability as a Measure of Potential Durability of Concrete Development of a Suitable Test Apparatus"; ACI Special Publication; SP 108.
12. Janes; "All the World's Aircraft"; 1988 - 1989, Janes Information Group Ltd. Surrey, UK (1988)
13. Schneider, U. and Diederichs, U.; "Detection of Cracks by Mercury Penetration Measurements"; in 'Fracture Mechanics of Concrete'; F.H.Wittmann (Editor); Elsevier; Amsterdam (1983)

14. Hinrichsmeyer, K.; "Analysis of Thermal Damage of Concrete by Application of a Structural Model"; in 'Forschungsarbeiten 1984-1989'; Institut fur Baustoffe, Massivbau und Brandschutz; Universtitaet Braunschweig, Heft 87 (1989)
15. Wu, G.Y.; "The Effect of Jet Fuel, Hydraulic Fluid and Cyclic Heating on Concrete Pavement"; Technical Memorandum No. 53-88-11; Port Hueneme; CA (1988)
16. Department of Defense; MIL-HDBK-1021/4 (1987)
17. Wu, G. Y., "Protective Coatings for F/A 18 Airfield Pavement", Tech. Memorandum No. 53-88-15; Port Hueneme, CA (1988).
18. Mehta, P. K., "CONCRETE Structure, Properties and Materials", p. 89, Prentice Hall Inc., Englewood Cliffs, NJ, (1986).

APPENDIX

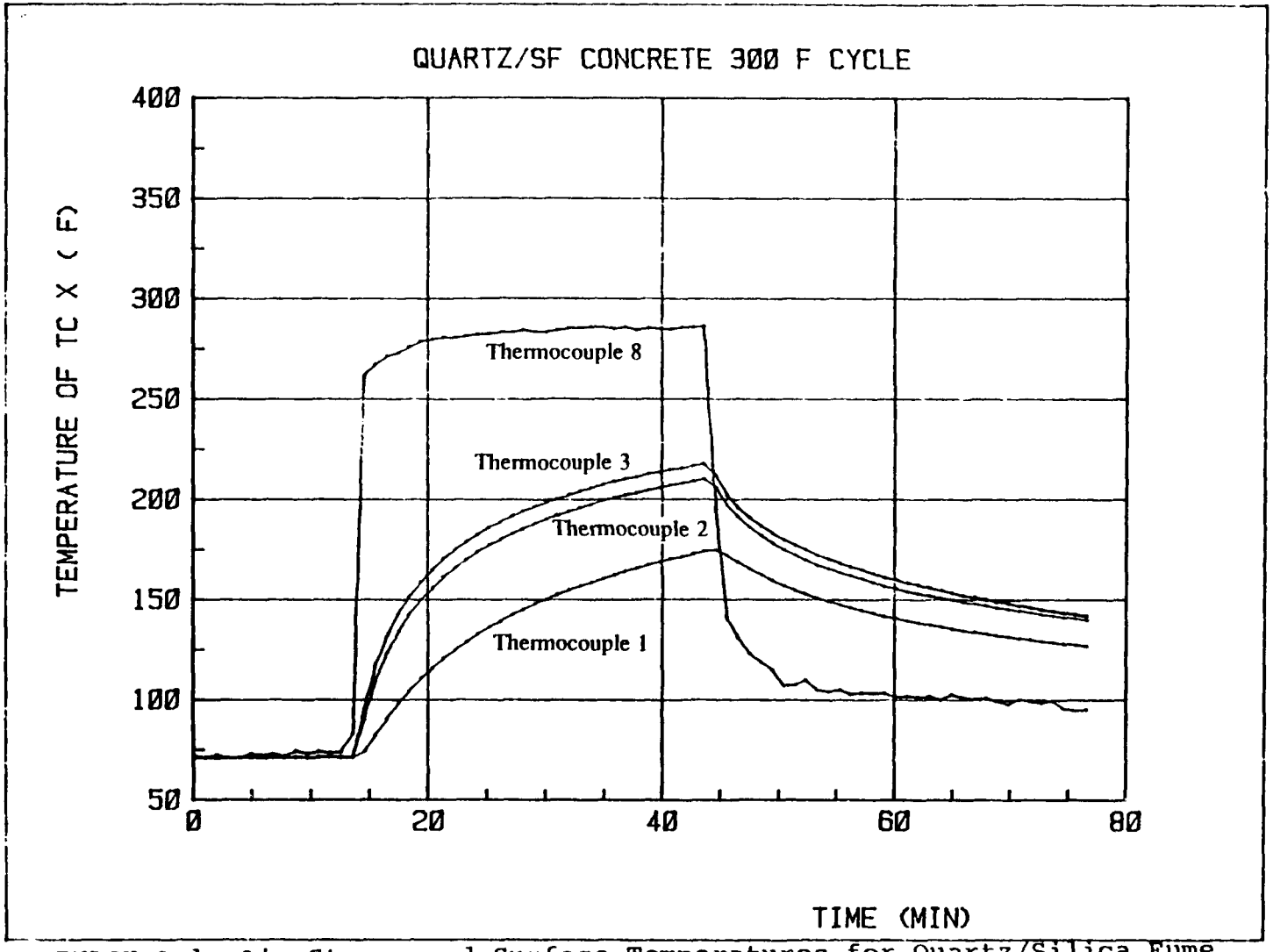

APPENDIX A-1 Air Stream and Surface Temperatures for Quartz/Silica Fume Concrete in Slab Test with Oven at 300F

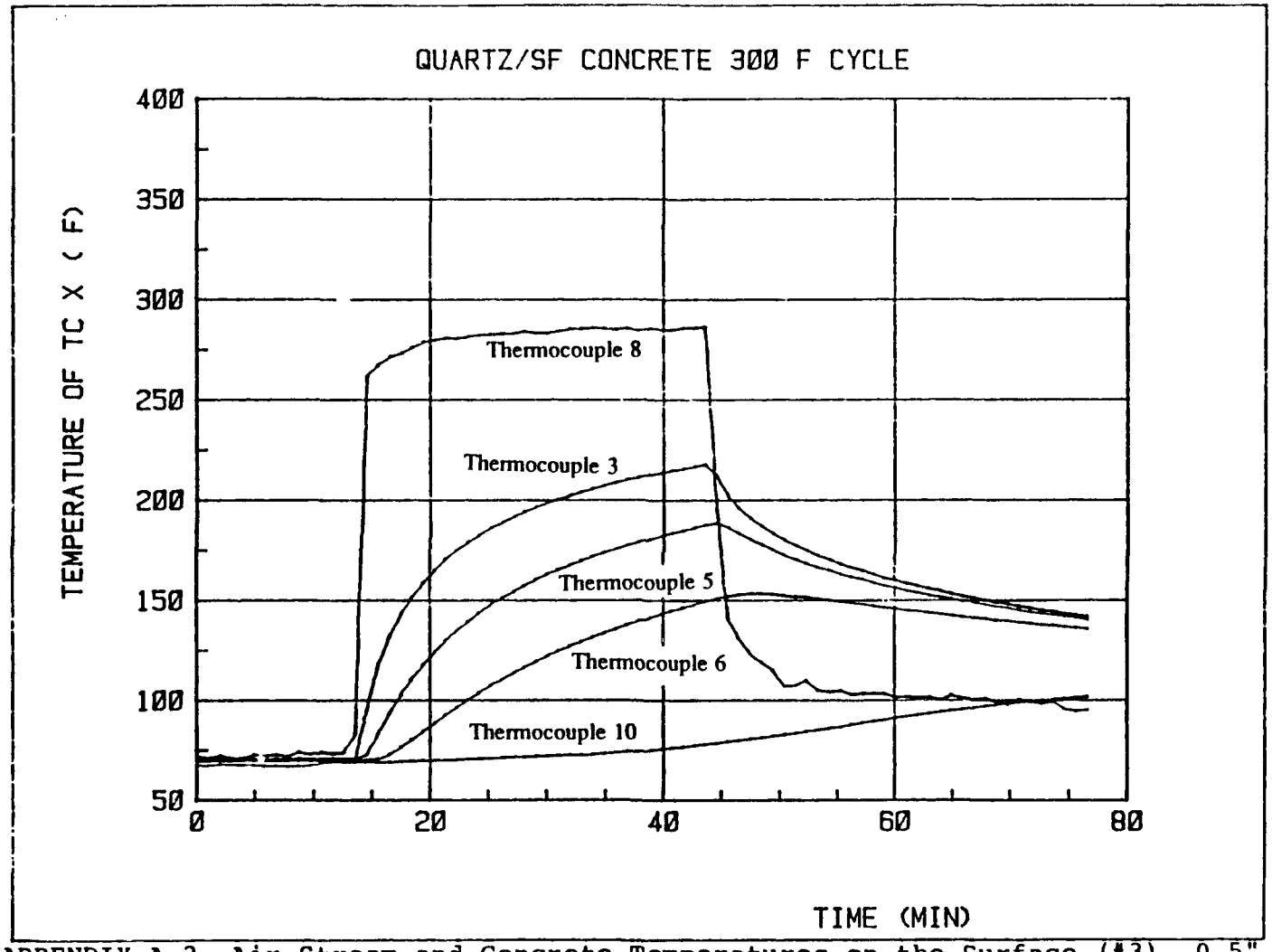

APPENDIX A-2 Air Stream and Concrete Temperatures on the Surface (#3), 0.5" below the Surface (#5), 1" below the Surface (#6) and on the Back Side of the Quartz/Silica Fume Concrete in Slab Test with Oven at 300F

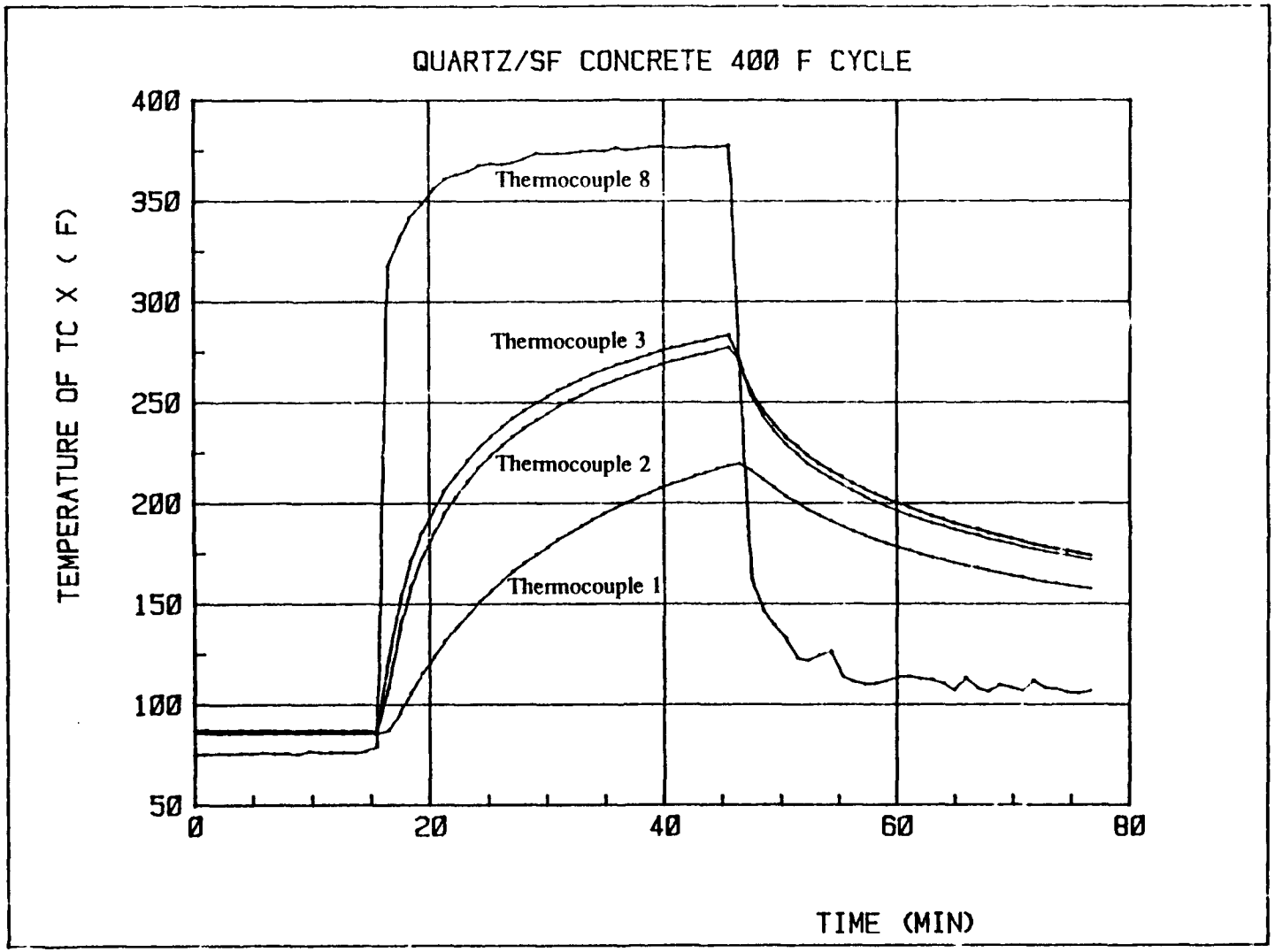

APPENDIX A-3 Air Stream and Surface Temperatures for Quartz/Silica Fume Concrete in Slab Test with Oven at 400F

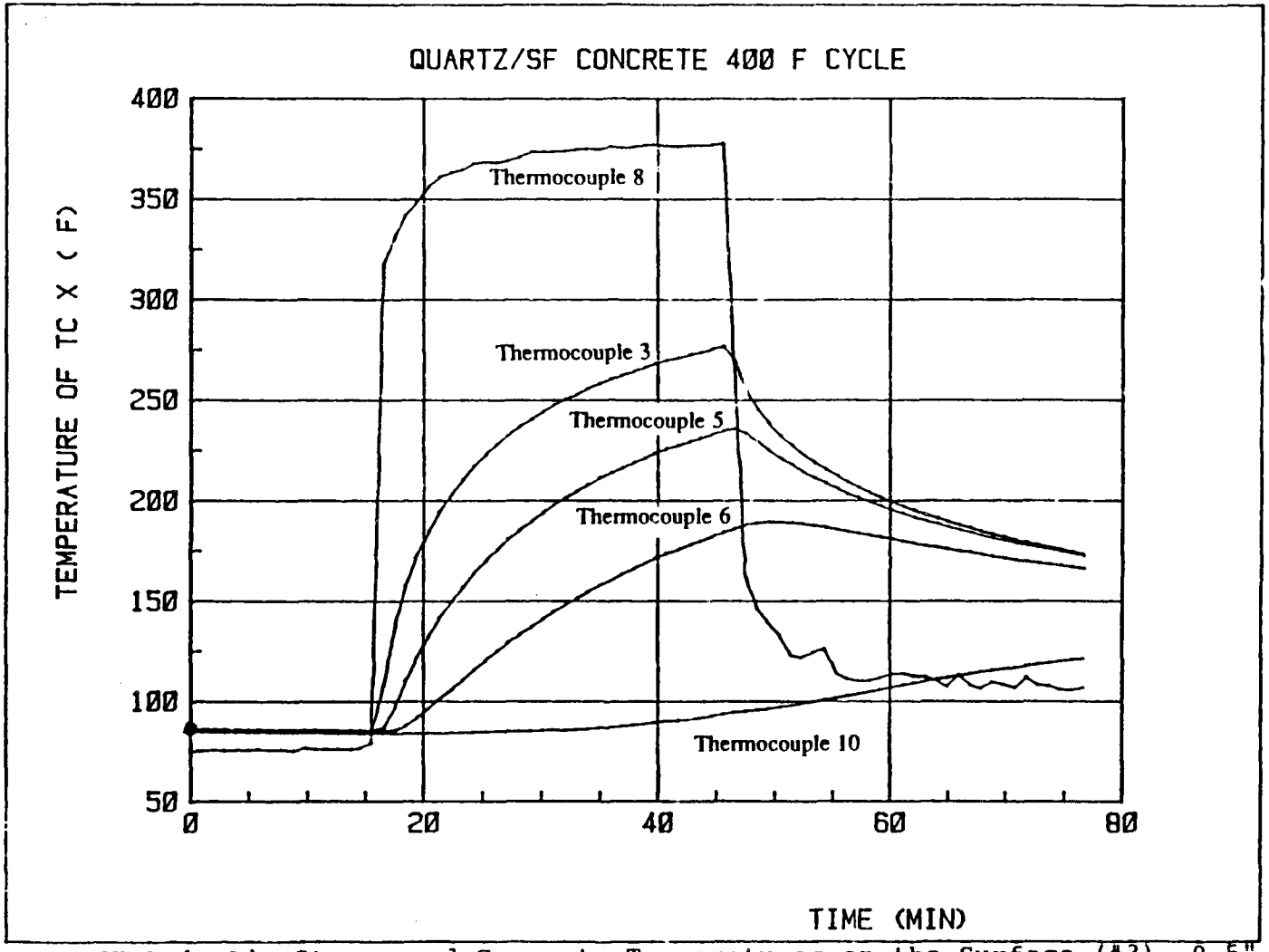

APPENDIX A-4 Air Stream and Concrete Temperatures on the Surface (#3), 0.5" Below the Surface (#5), 1" Below the Surface (#6) and the Back Side of the Quartz/Silica Fume Concrete in the Slab Test with Oven at 400F

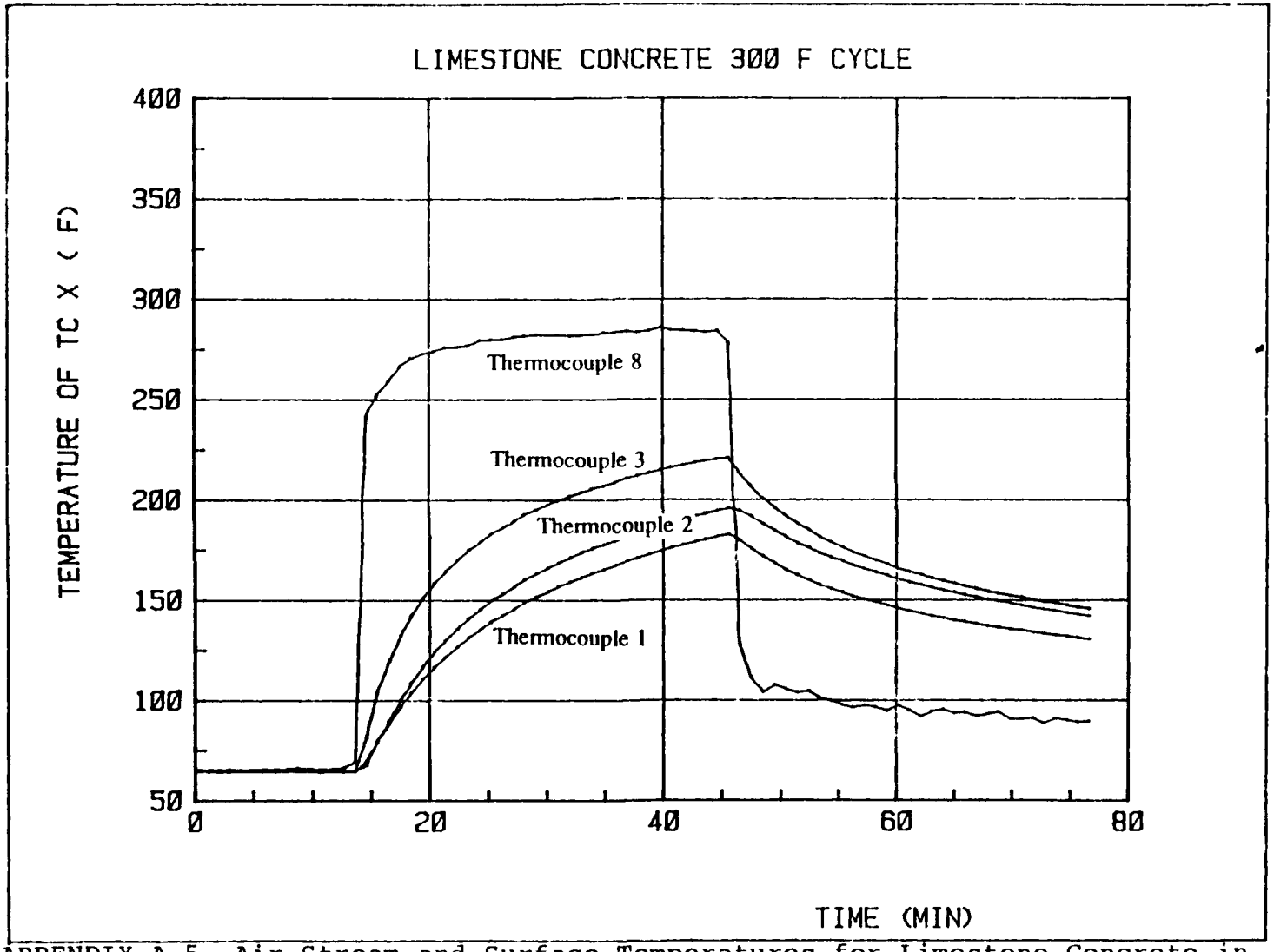

APPENDIX A-5 Air Stream and Surface Temperatures for Limestone Concrete in Slab Test with Oven at 300F

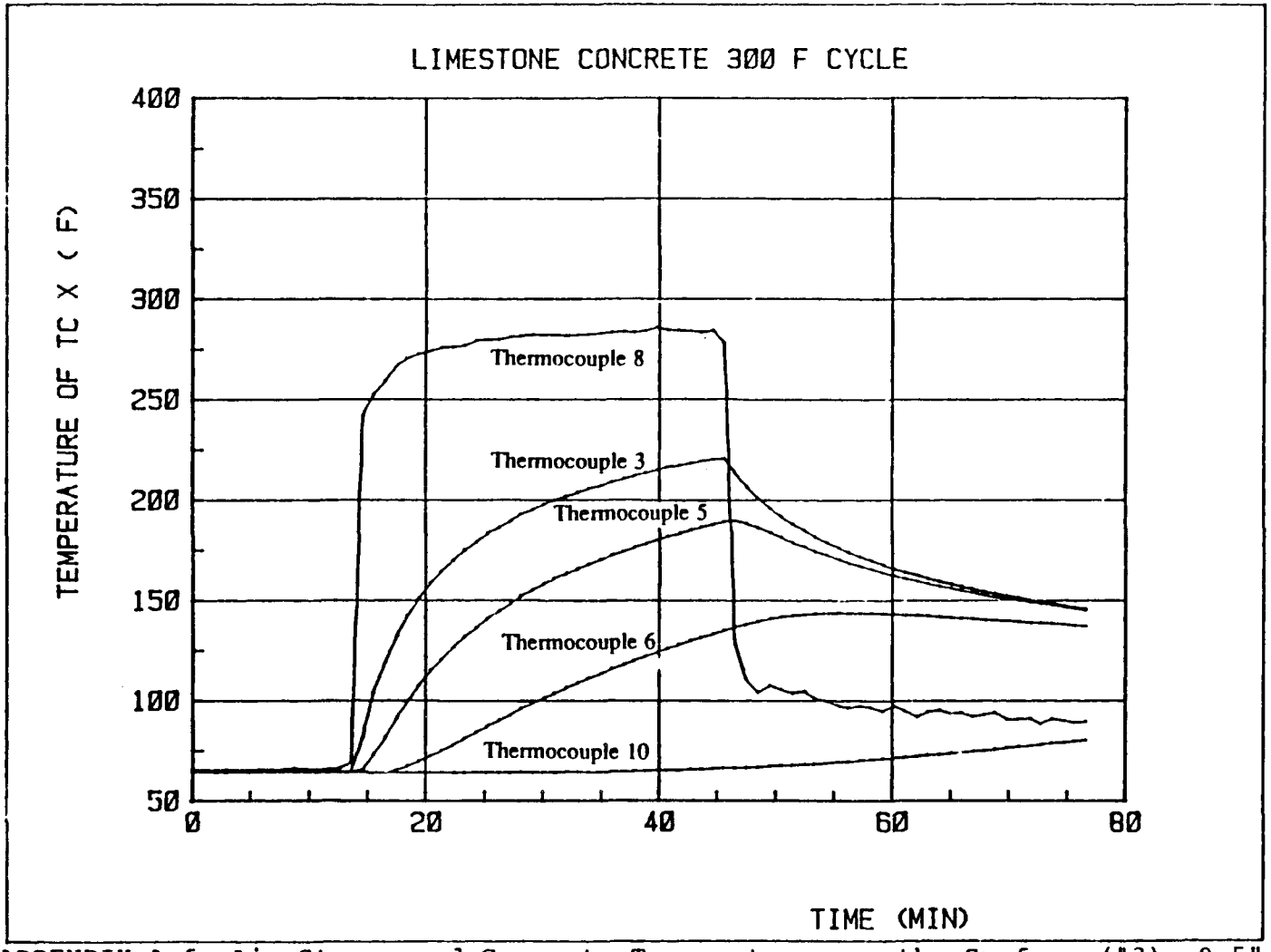

APPENDIX A-6 Air Stream and Concrete Temperatures on the Surface (#3), 0.5" Below the Surface (#5), 1" Below the Surface (#6) and on the Back Side of the Limestone Concrete in the Slab Test with the Oven at 300F

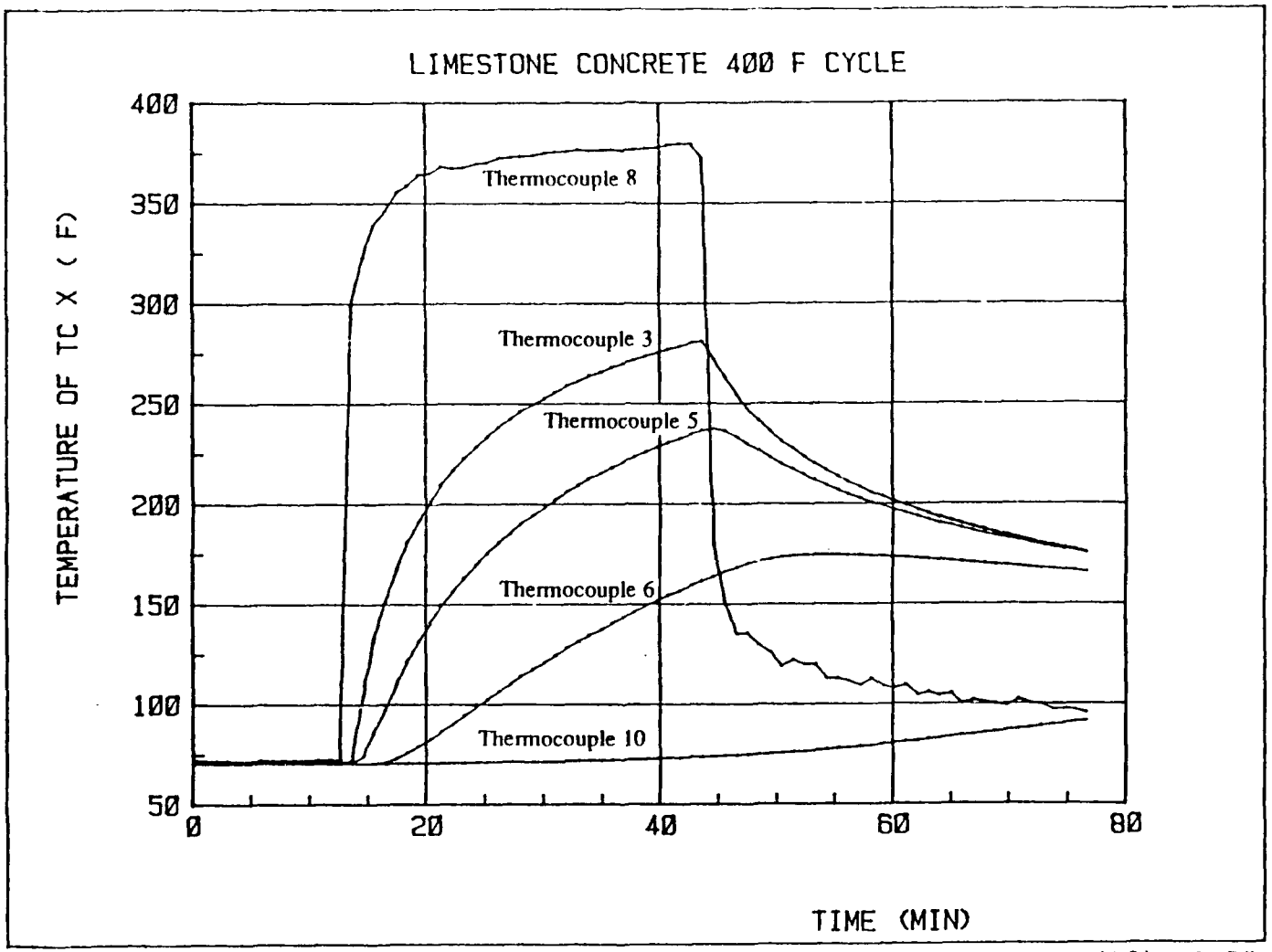

APPENDIX A-7 Air Stream and Concrete Temperatures on the Surface (#3), 0.5" Below the Surface (#5), 1" Below the Surface (#6) and the Back Side of the Limestone Concrete in the Slab Test with the Oven at 400F

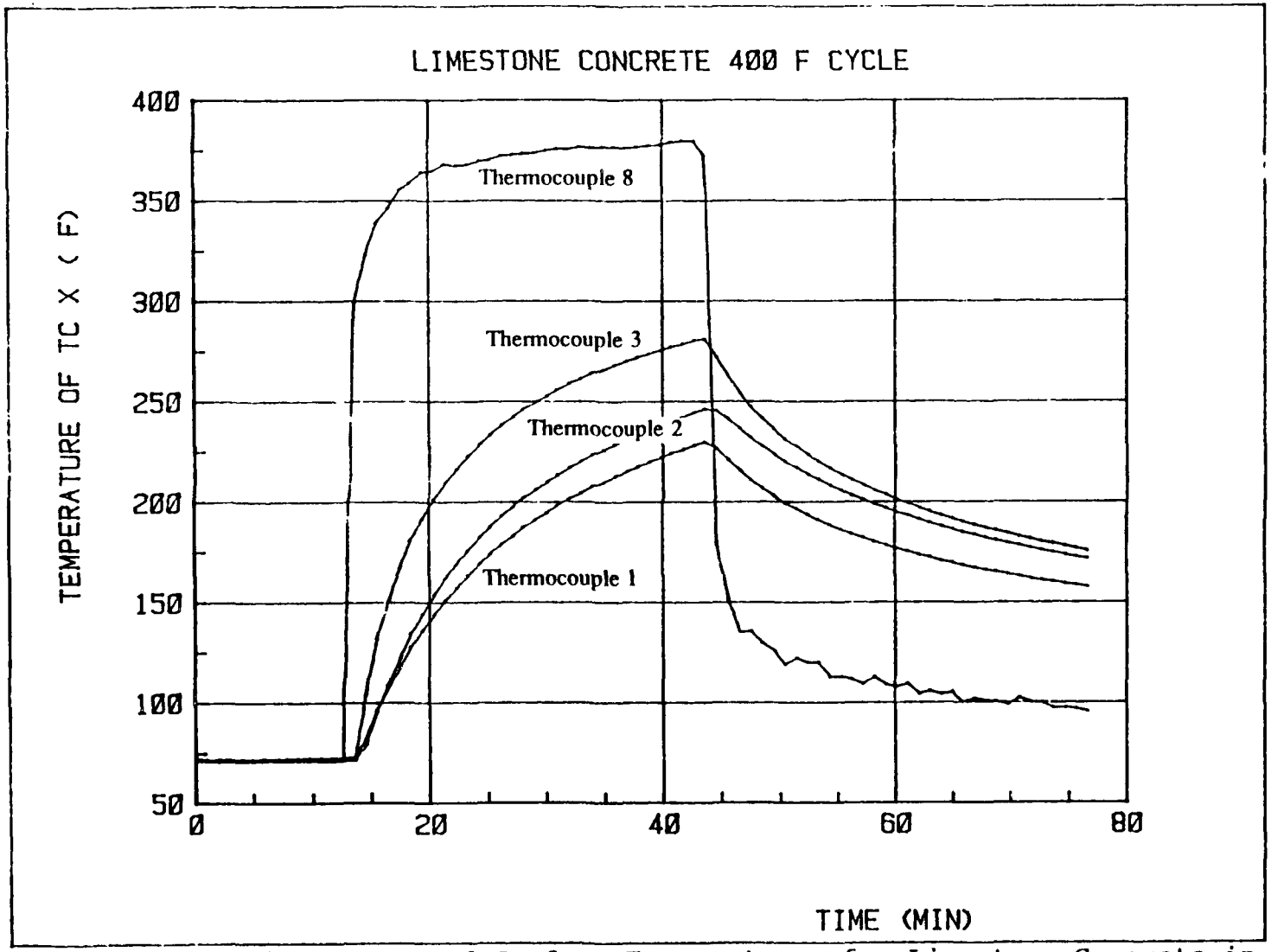

APPENDIX A-8 Air Stream and Surface Temperatures for Limestone Concrete in Slab Test with the Oven at 400F

Appendix A-9 Calculated stresses in limestone concrete after 30 minutes of convective heating from the F/A 18 APU using thermal expansion only. (negative values are compressive).

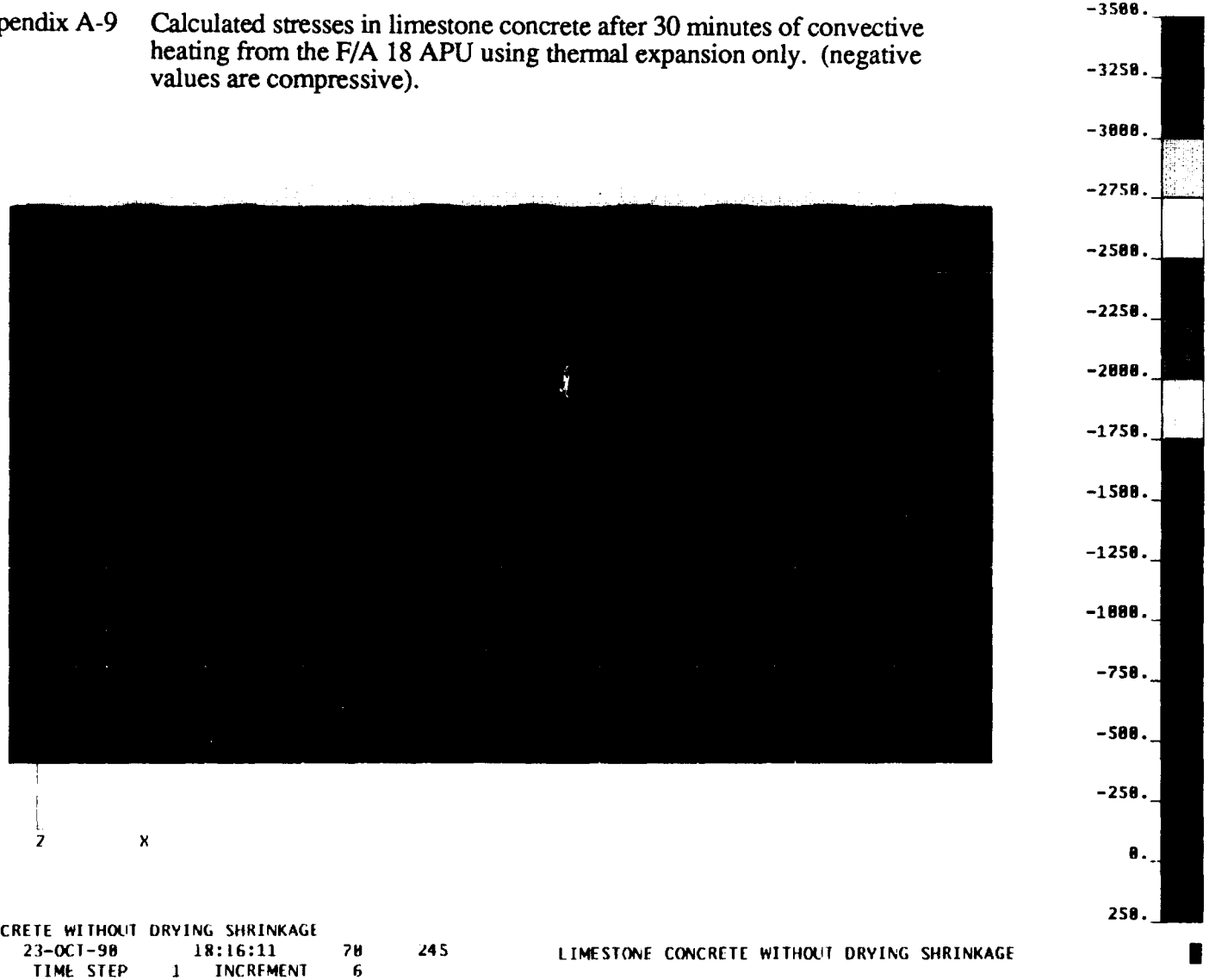

Appendix A-10 Calculated stresses in limestone concrete after 30 minutes of convective heating from the F/A 18 APU using thermal expansion and drying shinkage. (negative values are compressive).

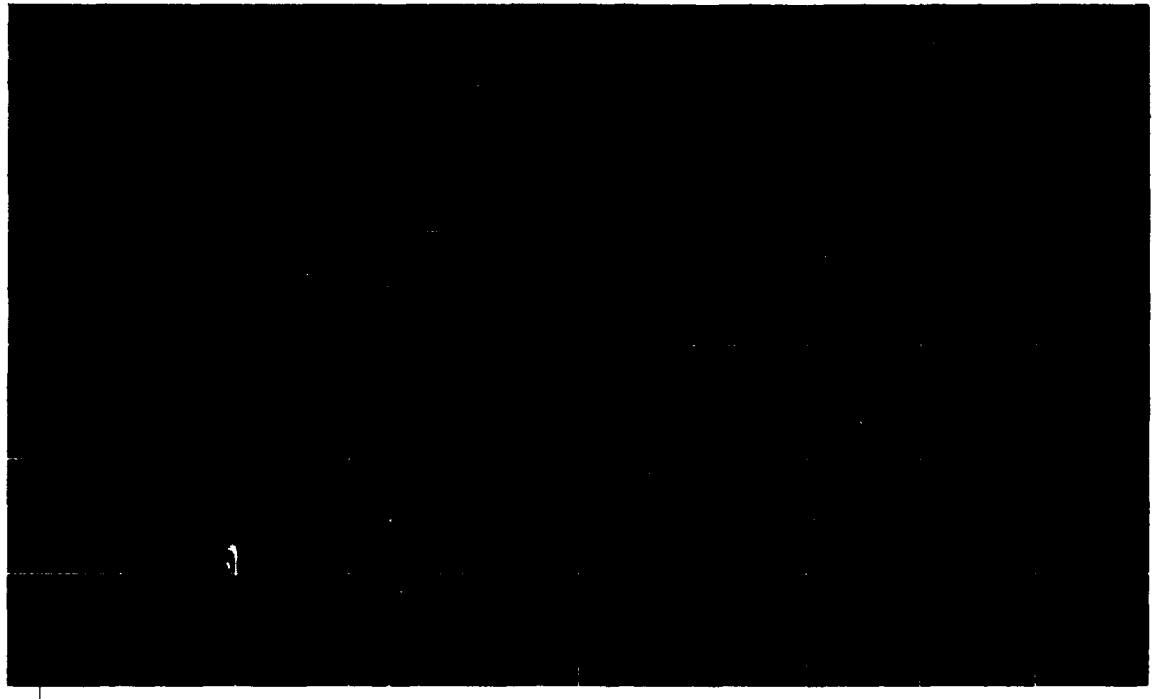

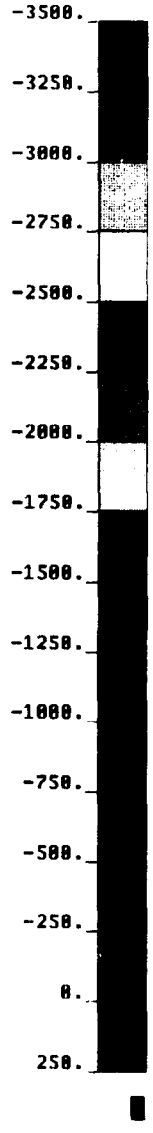

LIMESTONE CONCRETE WITHOUT DRYING SHRINKAGE
ABAQUS V4-8-4 1-NOV-90 17:08:50 70 245
PROCEDURE 21 TIME STEP 1 INCREMENT 10

LIMESTONE CONCRETE WITH DRYING SHRINKAGE

Appendix A-11 Calculated stresses in limestone concrete due to permanent shrinkage after convective heating then cooling (positive values are tensile).

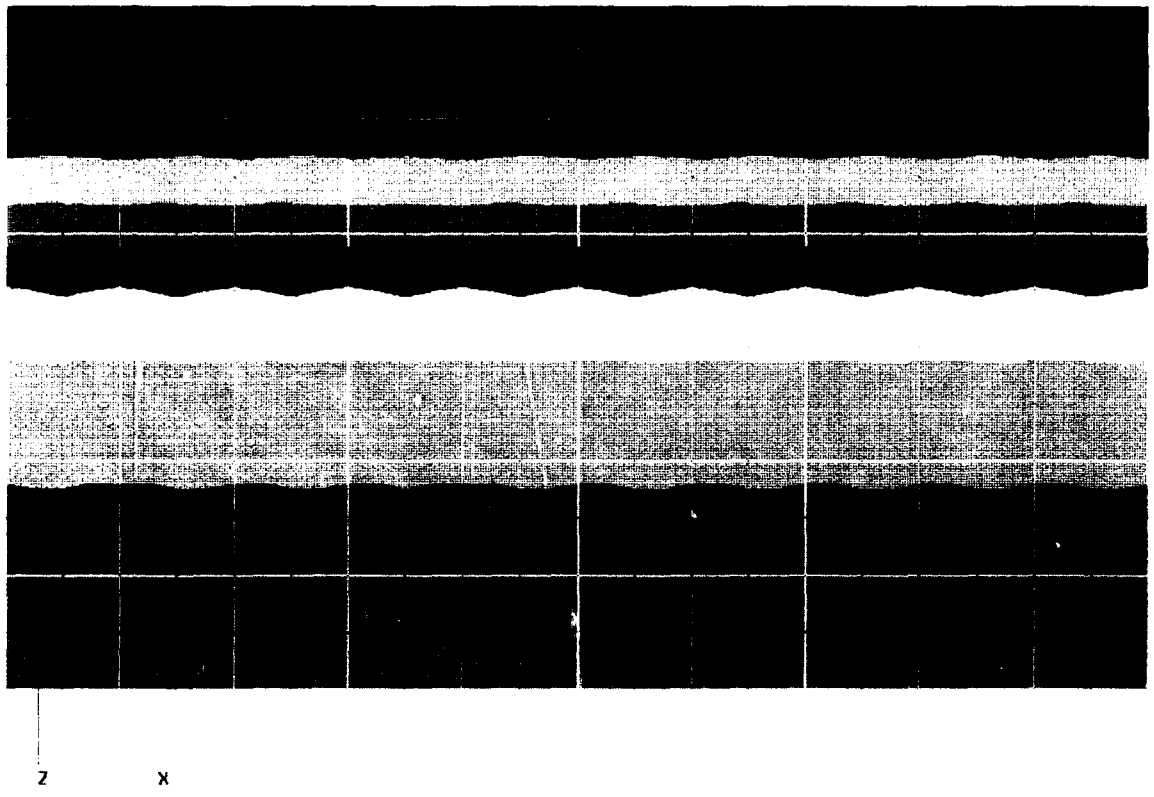

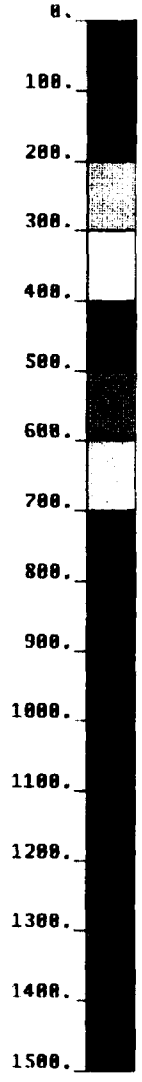

LIMESTONE CONCRETE WITHOUT DRYING SHRINKAGE
ABAQUS V4-8-4 1-NOV-90 17:38:59 70 245
PROCEDURE 1 TIME STEP 1 INCREMENT 6

LIMESTONE CONCRETE WITH PERMANENT SHRINKAGE

Appendix A-12 Calculated stresses in qurartz concrete after 30 minutes of convective heating from the F/A 18 APU using thermal expansion only. (negative values are compressive).

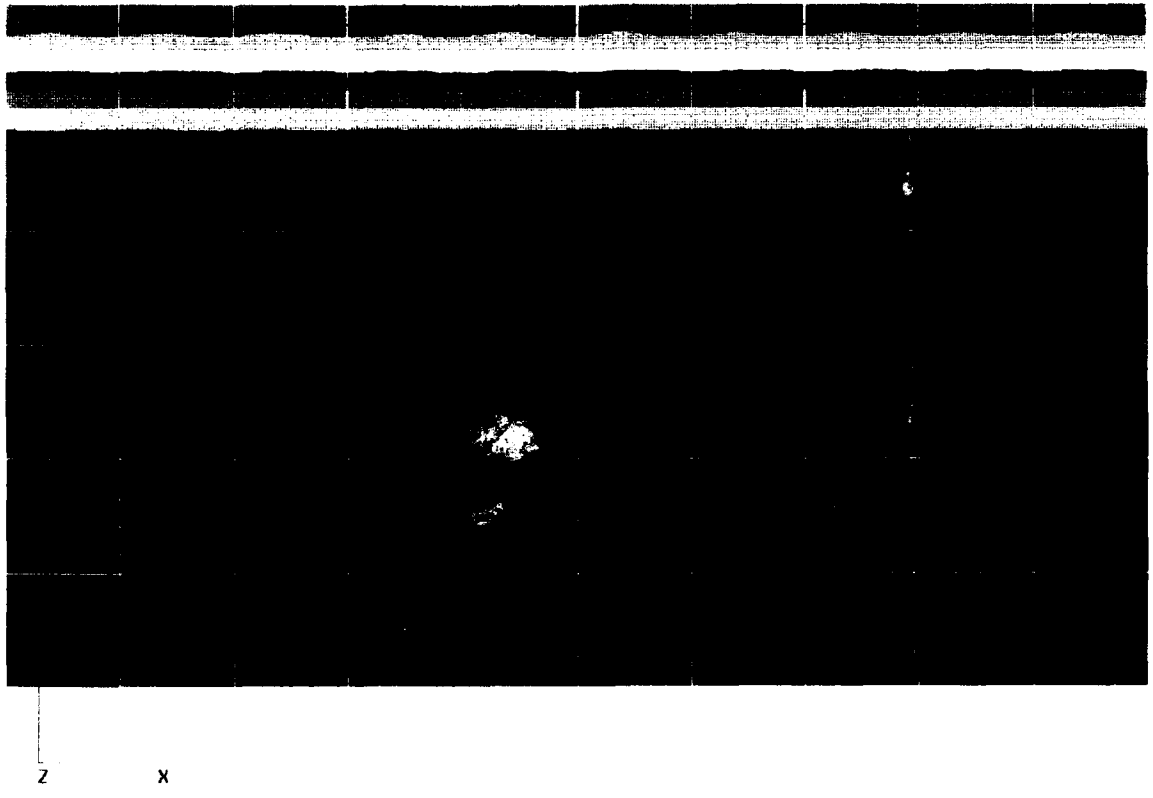

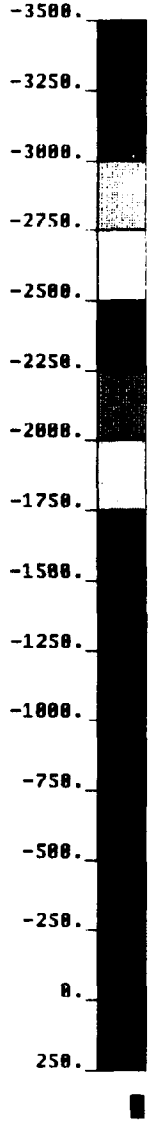

LIMESTONE CONCRETE WITHOUT DRYING SHRINKAGE
ABAQUS V4-8-4 24-OCT-90 15:11:33 78 245
PROCEDURE 1 TIME STEP 1 INCREMENT 6

QUARTZ CONCRETE WITHOUT DRYING SHRINKAGE

Appendix A-13 Calculated stresses in quartz concrete after 30 minutes of convective heating from the F/A 18 APU using thermal expansion and drying shinkage. (negative values are compressive).

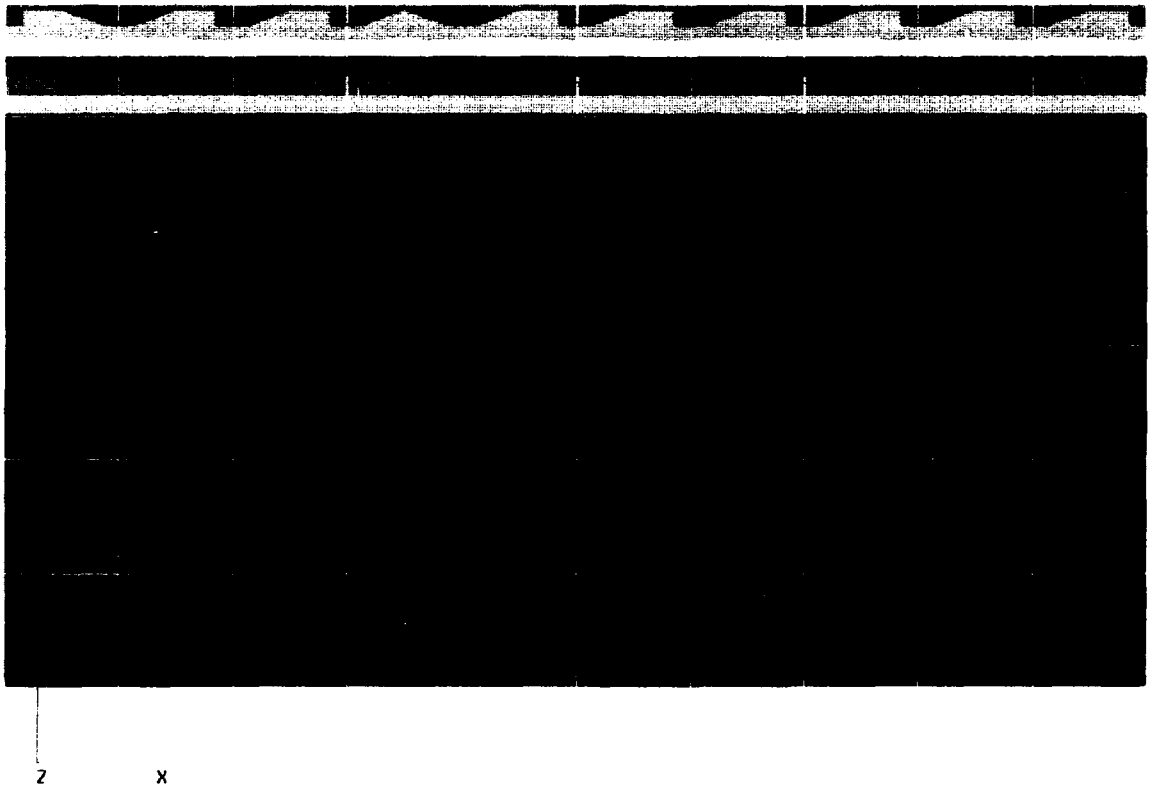

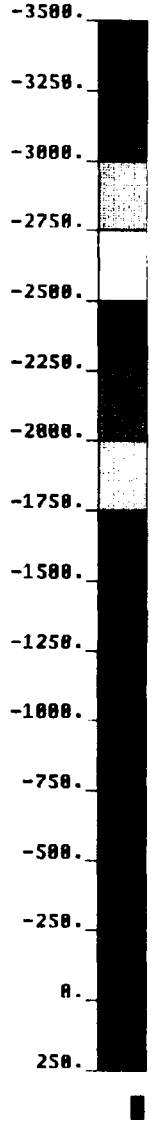

LIMESTONE CONCRETE WITHOUT DRYING SHRINKAGE
ABAQUS V4-8-4 1-NOV-90 16:56:27 70 245
PROCEDURE 21 TIME STEP 1 INCREMENT 10

QUARTZ CONCRETE WITH DRYING SHRINKAGE

Appendix A-14 Calculated stresses in quartz concrete due to permanent shrinkage after convective heating then cooling (positive values are tensile).

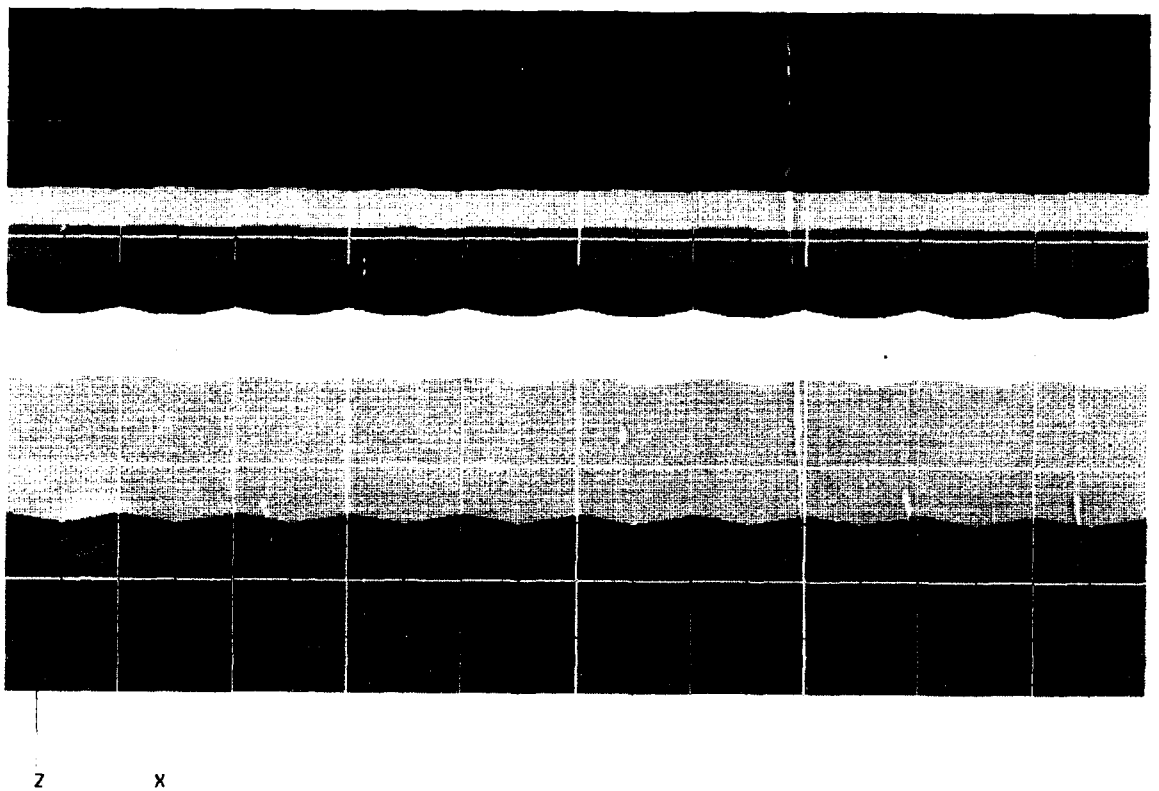

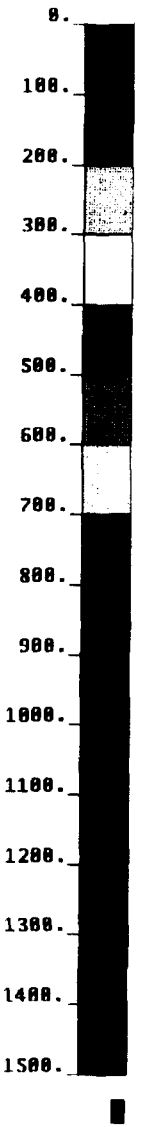

LIMESTONE CONCRETE WITHOUT DRYING SHRINKAGE
ABAQUS V4-8-4 1-NOV-90 17:58:12 70 245
PROCEDURE 1 TIME STEP 1 INCREMENT 6

QUARTZ CONCRETE WITH PERMANENT SHRINKAGE

Appendix A-15 Calculated stresses in quartz/silica fume concrete after 30 minutes of convective heating from the F/A 18 APU using thermal expansion only. (negative values are compressive).

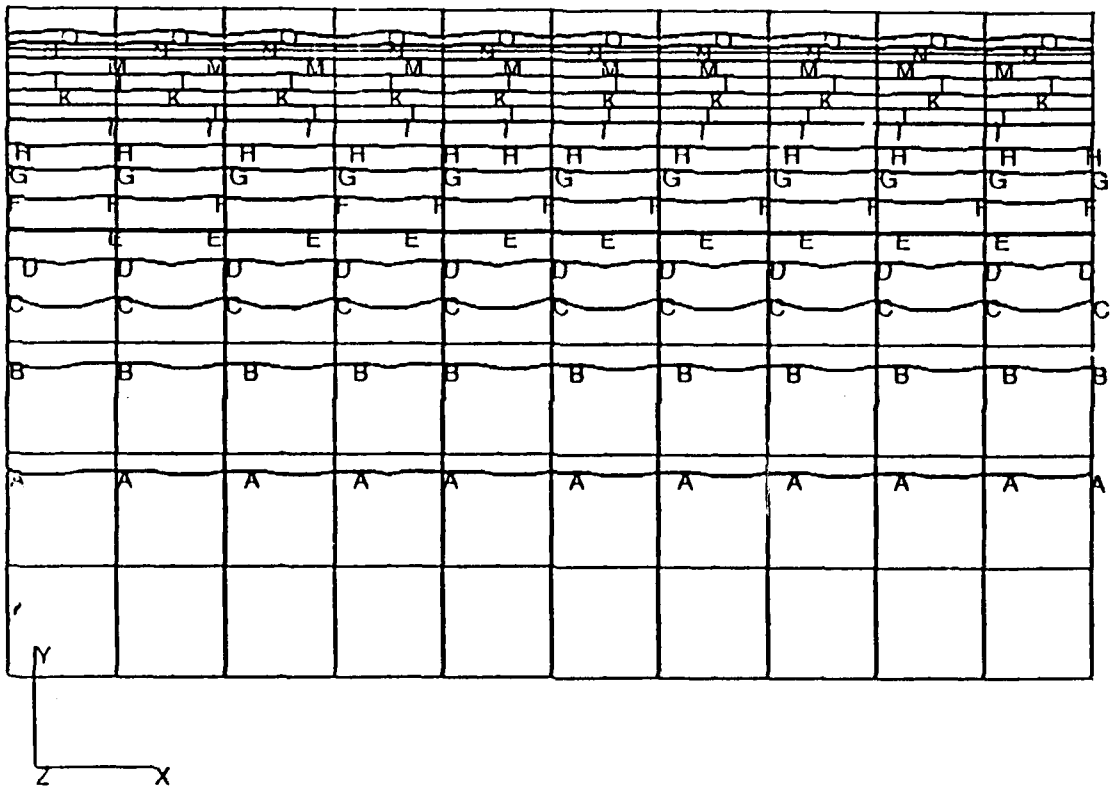

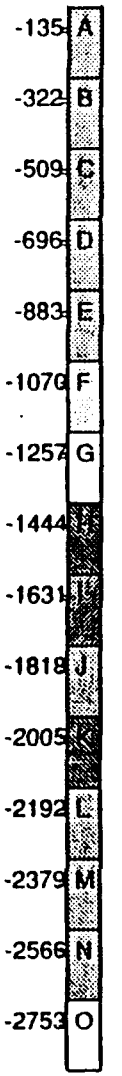

LIMESTONE CONCRETE WITHOUT DRYING SHRINKAGE
ABAQUS V4-8-4 28-NOV-90 15:41:35 70
PROCEDURE 21 TIME STEP 1 INCREMENT 10

Appendix A-16 Calculated stresses in quartz/silica fume concrete due to permanent shrinkage after convective heating then cooling (positive values are tensile).

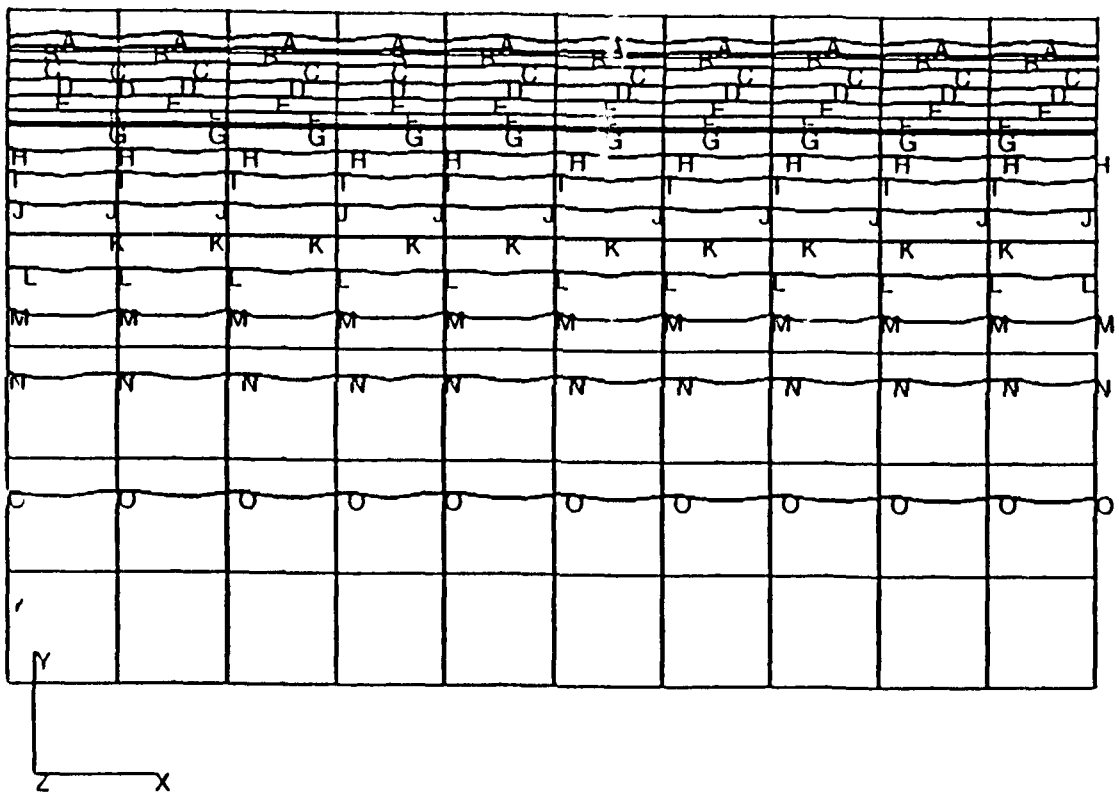

LIMESTONE CONCRETE WITHOUT DRYING SHRINKAGE
ABAQUS V4-8-4 28-NOV-90 15:58:45 70 245
PROCEDURE 1 TIME STEP 1 INCREMENT 6

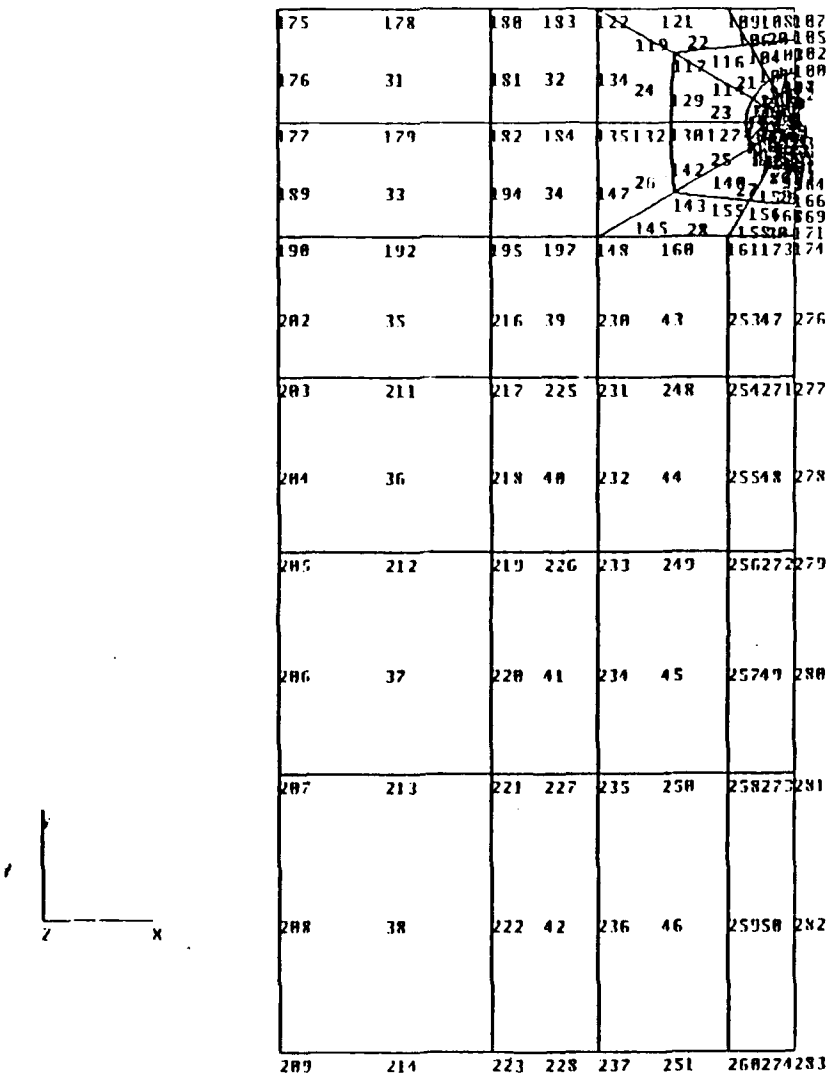

Appendix A-17 Finite element model of aggregate/matrix interaction.

FINITE ELEMENT MESH

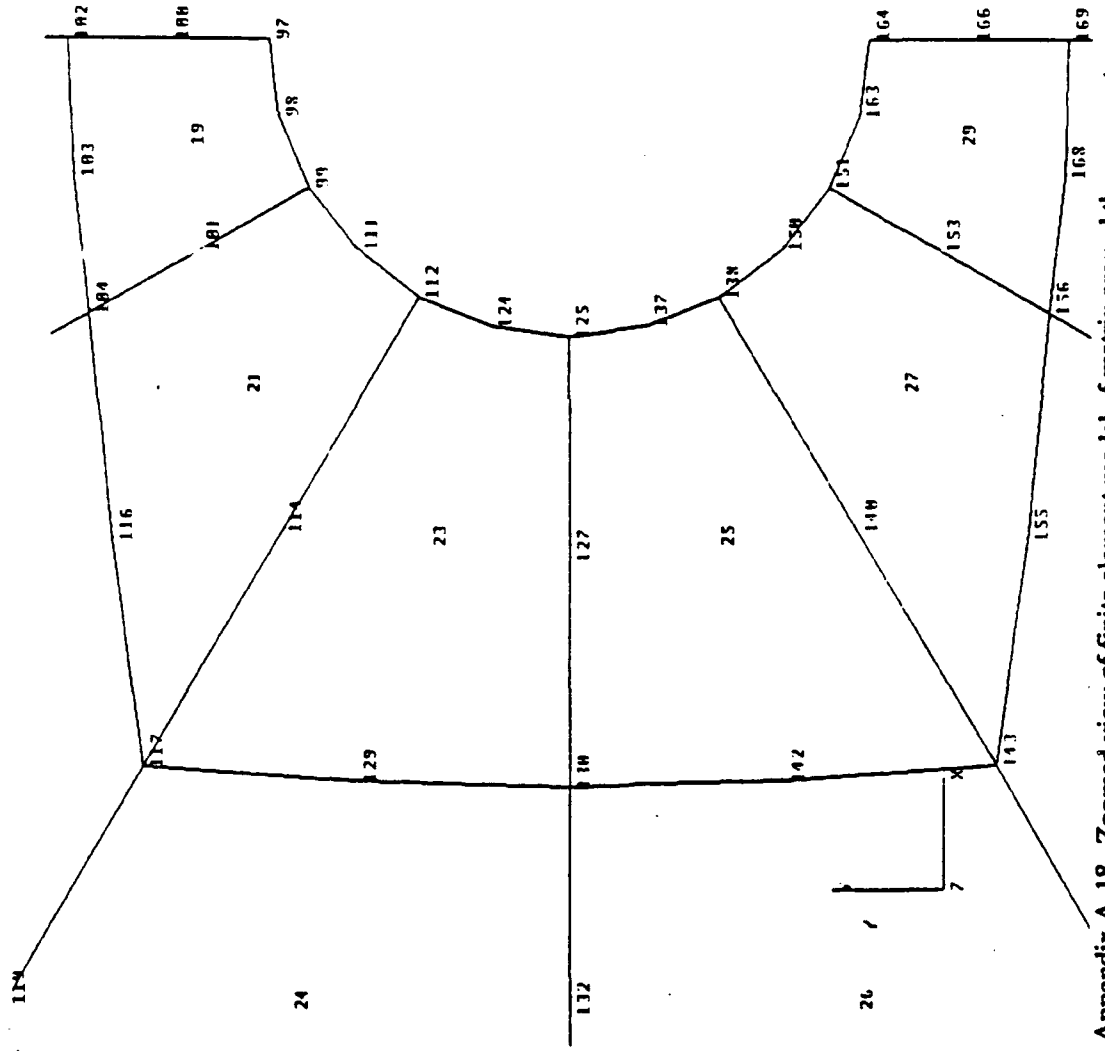

Appendix A-18 Zoomed view of finite element model of matrix around the aggregate.

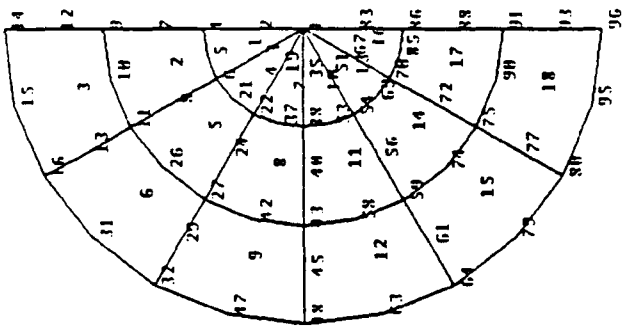

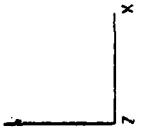

Appendix A-19 Zoomed view of finite element model of aggregate.

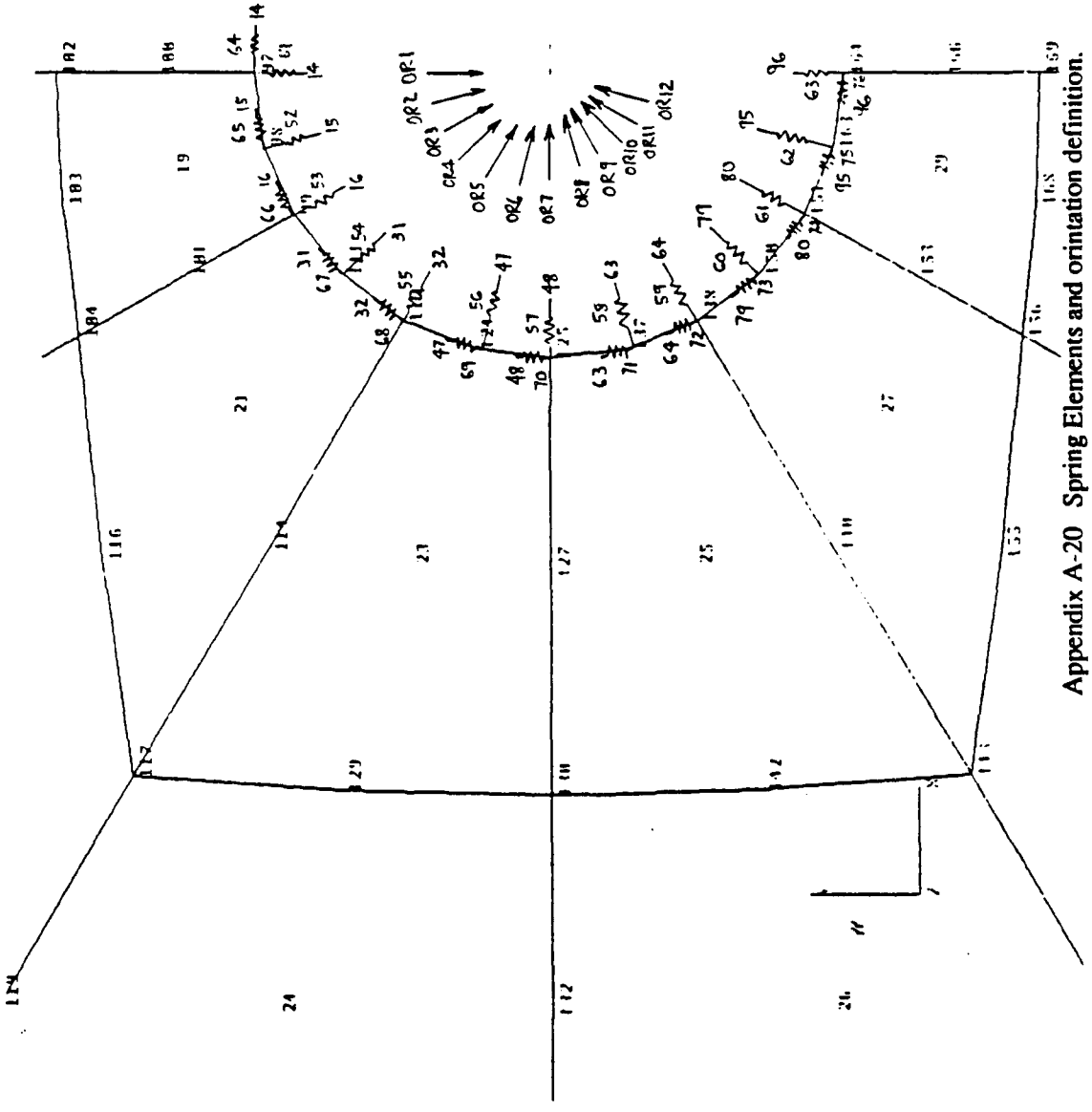

Appendix A-20 Spring Elements and orintation definition.

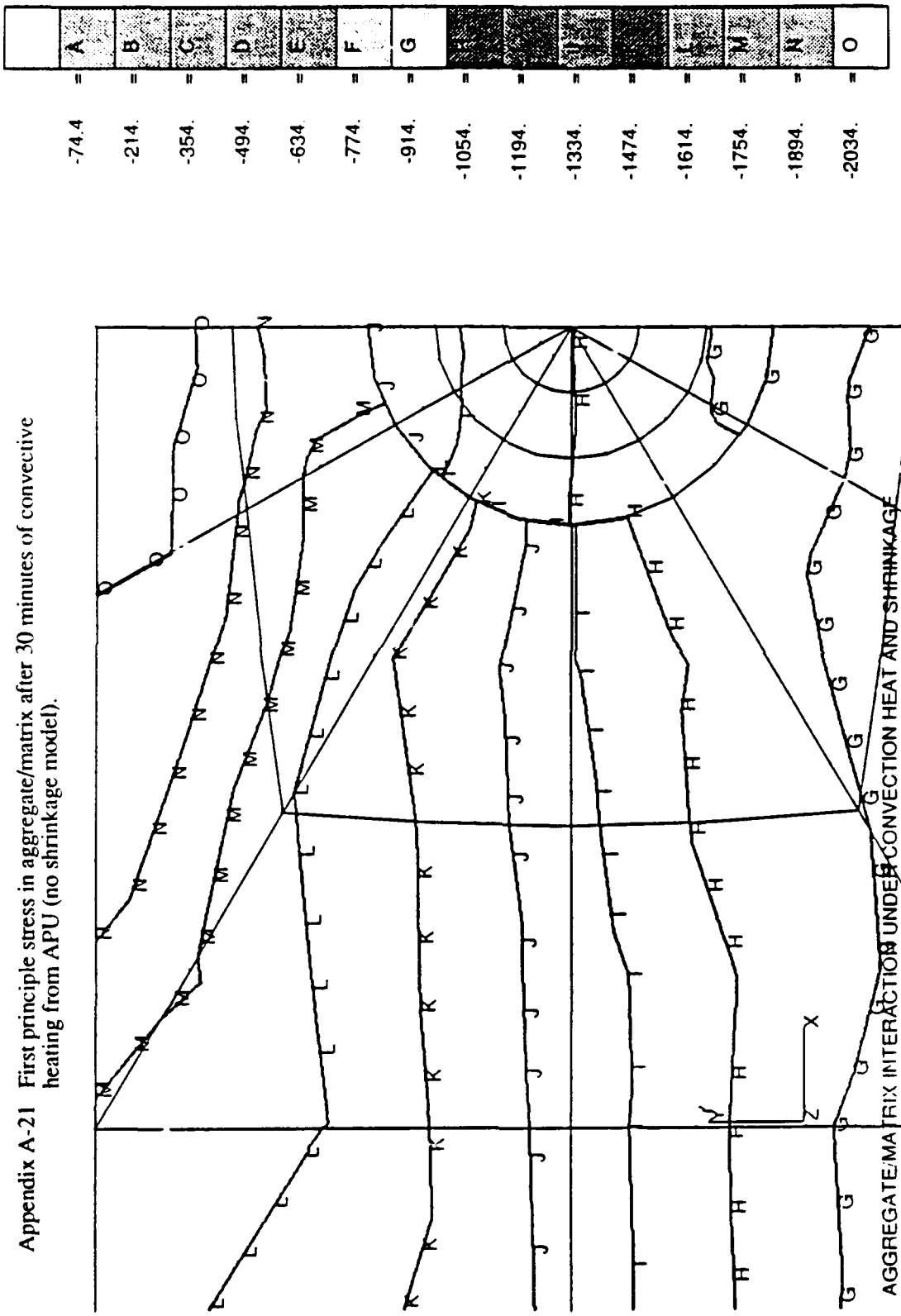

Appendix A-21 First principle stress in aggregate/matrix after 30 minutes of convective heating from APU (no shrinkage model).

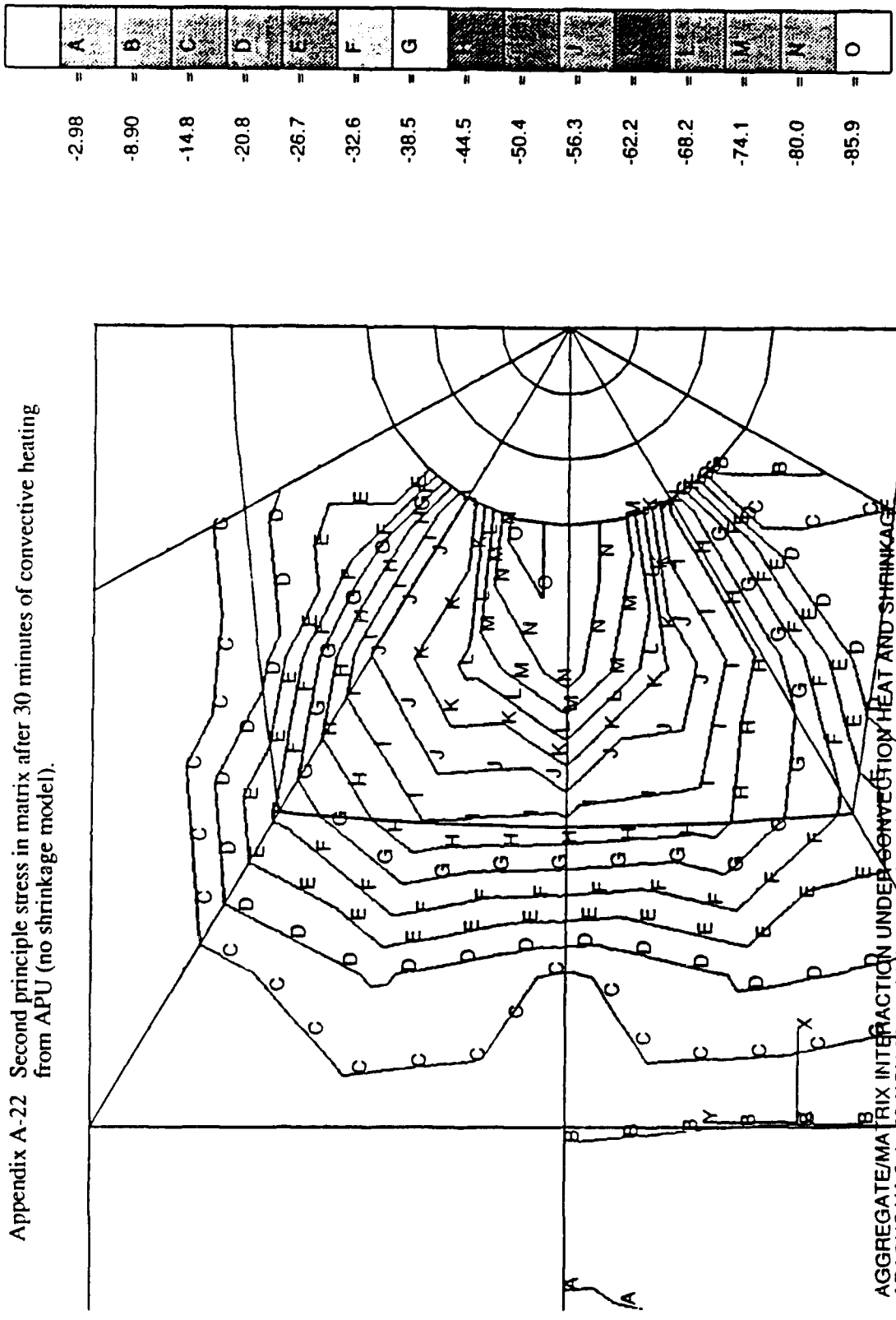

Appendix A-22 Second principle stress in matrix after 30 minutes of convective heating from APU (no shrinkage model).

Appendix A-23 Second principle stress in aggregate after 30 minutes of convective heating from APU (no shrinkage model).

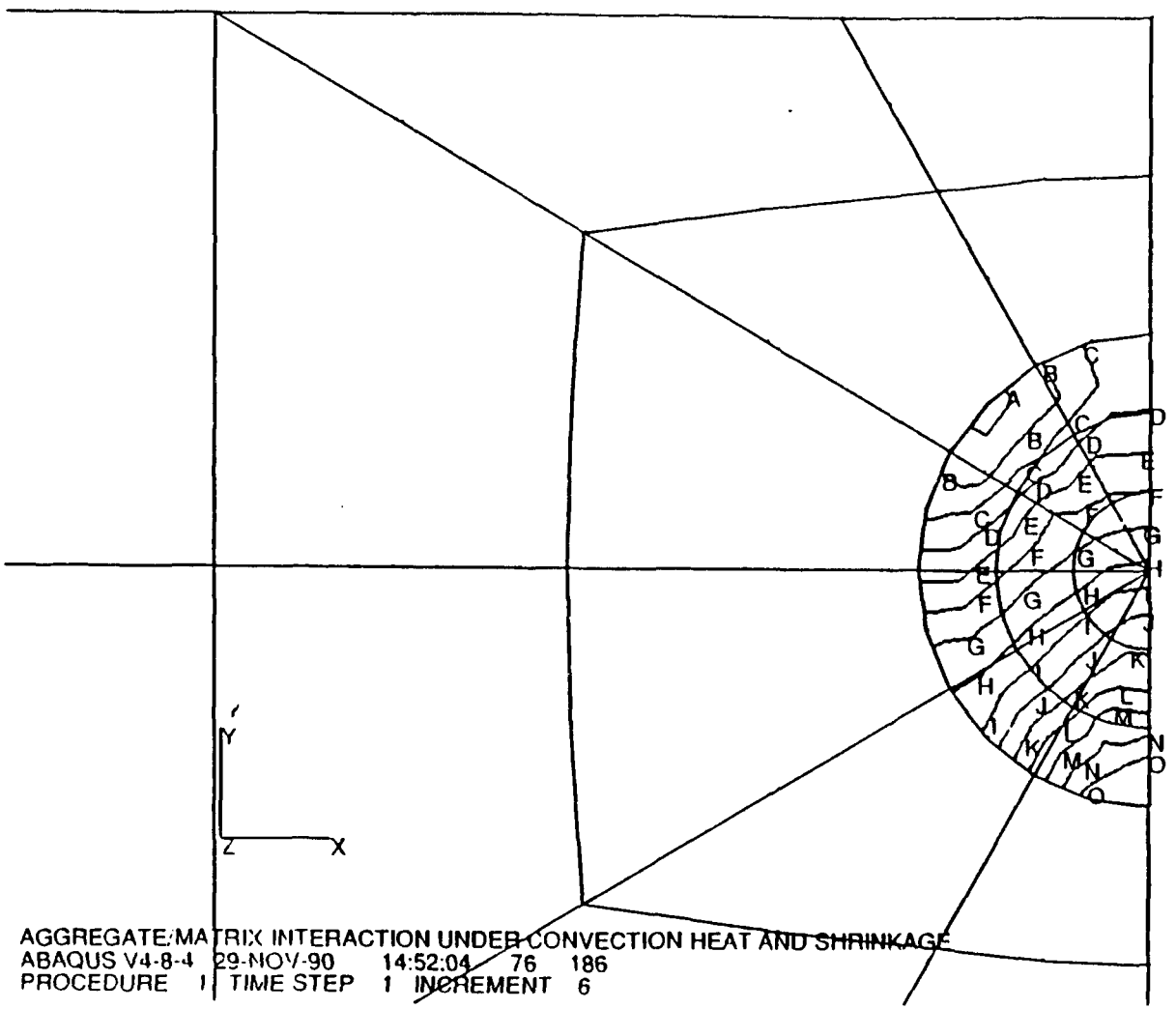

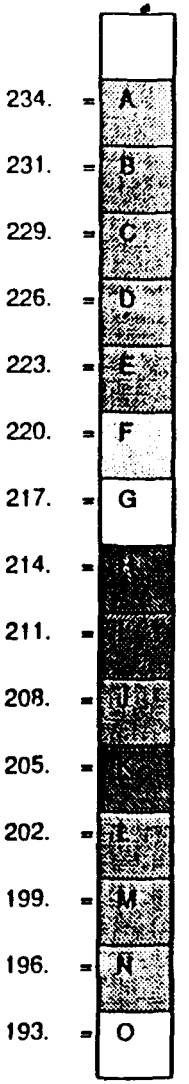

AGGREGATE/MATRIX INTERACTION UNDER CONVECTION HEAT AND SHRINKAGE
ABAQUS V4-8-4 29-NOV-90 14:52:04 76 186
PROCEDURE 1 TIME STEP 1 INCREMENT 6

DISTRIBUTION LIST

ARMY CERL / LIB, CHAMPAIGN, IL
ARMY CRREL / CRREL-IC, HANOVER, NH
DTIC / ALEXANDRIA, VA
FAA / ARD 200, WASHINGTON, DC
HQ AFESC / MANZIONE, TYNDALL AFB, FL; MURFEE, TYNDALL AFB, FL
NAVFACENGCOM / CODE 03, ALEXANDRIA, VA; CODE 03T, ALEXANDRIA, VA; CODE 04, ALEXANDRIA, VA; CODE 04A4, ALEXANDRIA, VA; CODE 04AB, ALEXANDRIA, VA; CODE 04B, ALEXANDRIA, VA; CODE 04B1 (M.P. JONES), ALEXANDRIA, VA; CODE 16, ALEXANDRIA, VA; CODE 163, ALEXANDRIA, VA; CODE 1632B, ALEXANDRIA, VA
NAVFACENGCOM LANTDIV / CODE 411, NORFOLK, VA; LIB, NORFOLK, VA
NAVFACENGCOM NORTHDIV / TECH LIB, PHILADELPHIA, PA
NAVFACENGCOM PACDIV / CODE 102, PEARL HARBOR, HI; CODE 405, PEARL HARBOR, HI
NAVFACENGCOM SOUTHDIV / CODE 102B, CHARLESTON, SC; CODE 4023, CHARLESTON, SC; LIB, CHARLESTON, SC
NAVFACENGCOM WESTDIV / CODE 411, SAN BRUNO, CA
NAVSCOLCECOFF / CODE C35, PORT HUENEME, CA
WES / LIBRARY, VICKSBURG, MS

DISTRIBUTION QUESTIONNAIRE

The Naval Civil Engineering Laboratory is revising its primary distribution lists.

SUBJECT CATEGORIES

1 SHORE FACILITIES
1A Construction methods and materials (including corrosion control, coatings)
1B Waterfront structures (maintenance/deterioration control)
1C Utilities (including power conditioning)
1D Explosives safety
1E Aviation Engineering Test Facilities
1F Fire prevention and control
1G Antenna technology
1H Structural analysis and design (including numerical and computer techniques)
1J Protective construction (including hardened shelters, shock and vibration studies)
1K Soil/rock mechanics
1L Airfields and pavements
1M Physical security

2 ADVANCED BASE AND AMPHIBIOUS FACILITIES
2A Base facilities (including shelters, power generation, water supplies)
2B Expedient roads/airfields/bridges
2C Over-the-beach operations (including breakwaters, wave forces)
2D POL storage, transfer, and distribution
2E Polar engineering

3 ENERGY/POWER GENERATION
3A Thermal conservation (thermal engineering of buildings, HVAC systems, energy loss measurement, power generation)
3B Controls and electrical conservation (electrical systems, energy monitoring and control systems)
3C Fuel flexibility (liquid fuels, coal utilization, energy from solid waste)
3D Alternate energy source (geothermal power, photovoltaic power systems, solar systems, wind systems, energy storage systems)
3E Site data and systems integration (energy resource data, integrating energy systems)
3F EMCS design

4 ENVIRONMENTAL PROTECTION
4A Solid waste management
4B Hazardous/toxic materials management
4C Waterwaste management and sanitary engineering
4D Oil pollution removal and recovery
4E Air pollution
4F Noise abatement

5 OCEAN ENGINEERING
5A Seafloor soils and foundations
5B Seafloor construction systems and operations (including diver and manipulator tools)
5C Undersea structures and materials
5D Anchors and moorings
5E Undersea power systems, electromechanical cables, and connectors
5F Pressure vessel facilities
5G Physical environment (including site surveying)
5H Ocean-based concrete structures
5J Hyperbaric chambers
5K Undersea cable dynamics

ARMY FEAP
BDG Shore Facilities
NRG Energy
ENV Environmental/Natural Responses
MGT Management
PRR Pavements/Railroads

TYPES OF DOCUMENTS

D = Techdata Sheets; **R** = Technical Reports and Technical Notes; **G** = NCEL Guides and Abstracts; **I** = Index to TDS; **U** = User Guides; ☐ None - remove my name

Old Address:

_____

_____

_____

_____

Telephone No.: _____

New Address:

_____

_____

_____

_____

Telephone No.: _____

INSTRUCTIONS

The Naval Civil Engineering Laboratory has revised its primary distribution lists. To help us verify our records and update our data base, please do the following:

- Add - circle number on list
- Remove my name from all your lists - check box on list.
- Change my address - add telephone number
- Number of copies should be entered after the title of the subject categories you select.
- Are we sending you the correct type of document? If not, circle the type(s) of document(s) you want to receive listed on the back of this card.

Fold on line, staple, and drop in mail.

DEPARTMENT OF THE NAVY

Naval Civil Engineering Laboratory
Port Hueneme, CA 93043-5003

Official Business
Penalty for Private Use, $300

NO POSTAGE NECESSARY IF MAILED IN THE UNITED STATES

BUSINESS REPLY CARD

FIRST CLASS PERMIT NO. 12503 WASH D.C.

POSTAGE WILL BE PAID BY ADDRESSEE

CODE L34 (J LEDERER)
COMMANDING OFFICER
NAVAL CIVIL ENGINEERING LABORATORY
PORT HUENEME CA 93043-5003

NCEL DOCUMENT EVALUATION

You are number one with us; how do we rate with you?

We at NCEL want to provide you our customer the best possible reports but we need your help. Therefore, I ask you to please take the time from your busy schedule to fill out this questionnaire. Your response will assist us in providing the best reports possible for our users. I wish to thank you in advance for your assistance. I assure you that the information you provide will help us to be more responsive to your future needs.

R. N. STORER, Ph.D, P.E.
Technical Director

DOCUMENT NO. _____ TITLE OF DOCUMENT: _____

_____

Date: _____ Respondent Organization : _____

Name: _____ Activity Code: _____
Phone: _____ Grade/Rank: _____

Category (*please check*):

Sponsor ____ User ____ Proponent ____ Other (*Specify*) _____

Please answer on your behalf only; not on your organization's. Please check (*use an X*) only the block that most closely describes your attitude or feeling toward that statement:

SA Strongly Agree A Agree O Neutral D Disagree SD Strongly Disagree

---

	SA	A	N	D	SD
1. The technical quality of the report is comparable to most of my other sources of technical information.	( )	( )	( )	( )	( )
2. The report will make significant improvements in the cost and or performance of my operation.	( )	( )	( )	( )	( )
3. The report acknowledges related work accomplished by others.	( )	( )	( )	( )	( )
4. The report is well formatted.	( )	( )	( )	( )	( )
5. The report is clearly written.	( )	( )	( )	( )	( )
6. The conclusions and recommendations are clear and directly supported by the contents of the report.	( )	( )	( )	( )	( )
7. The graphics, tables, and photographs are well done.	( )	( )	( )	( )	( )

Do you wish to continue getting NCEL reports? ☐ YES ☐ NO

Please add any comments (e.g., in what ways can we improve the quality of our reports?) on the back of this form.

Comments:

Please fold on line and staple

DEPARTMENT OF THE NAVY

Naval Civil Engineering Laboratory
Port Hueneme, CA 93043-5003

Official Business
Penalty for Private Use $300

Code L03B
NAVAL CIVIL ENGINEERING LABORATORY
PORT HUENEME, CA 93043-5003